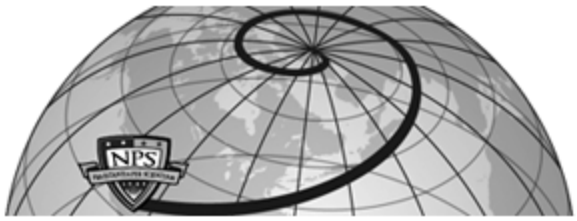

PROPERTIES OF HIGH CURRENT SUPERCONDUCTING MAGNET COILS

ROBERT H. FINLEY
and
RICHARD T. MARTIN

PROPERTIES OF HIGH CURRENT SUPERCONDUCTING MAGNET COILS

by

Robert H. Finley

and

Richard T. Martin

This work is accepted as fulfilling

the thesis requirements for the degree of

MASTER OF SCIENCE

IN

PHYSICS

from the

United States Naval Postgraduate School

ABSTRACT

In connection with the fabrication of an adiabatic demagnetization cooling device, the properties of some high current superconducting magnet coils have been studied. This thesis includes investigations of critical current vs. magnetic field for Nb_3Zr coils wound with several packing fractions. The coils were wound bifilar in order that conditions of zero net field could be studied, as well as the properties of single and multiple layers of windings. The problems of connections to the Nb_3Zr wire and the thermal expansion of the wire were investigated. An experiment was conducted to determine the optimum size current lead for various currents. A design is presented for a magnetic cooling device utilizing the magnet. Techniques have been developed for growing large single crystals or ferric ammonium sulfate alum for use with the device.

We wish to express many thanks to K. C. Smith, M. K. Andrews, L. F. May, R. C. Moeller, Professor O. B. Wilson, JR., and of course Professor E. C. Crittenden, Jr., for their invaluable assistance in this project.

TABLE OF CONTENTS

LIST OF ILLUSTRATIONS

List of Illustrations (Continued)

1. Introduction.

The original intent of the authors was to utilize a superconducting solenoid in an adiabatic demagnetization device. Appendices VI and VII of this work contains details on the cooling device and the paramagnetic salt used. However, since the primary unknowns were with the magnet, the bulk of the research and this report are concerned with it.

We have employed Niobium-Zirconium (Nb_3Zr) wire. Experiments have been conducted on the thermal expansion coefficient (See Appendix III) on means of making high current connections to the wire (See Appendix II), and on the effects of geometry of winding on the superconducting properties of this wire.

Two coils were wound for studying the properties of the magnet. Coil number one was wound bifilar (with respect to the superconducting wire) with taps at the end of each layer for studying various current and field configurations. Coil number two was also wound bifilar, but with taps only at the ends. This coil is intended for use with the cooling device.

We have observed that a relationship published by Montgomery /2/ for describing the difference between the short speciman performance and performance in a coil is insufficient to describe our data in instances when we were able to produce a zero field with opposing windings.

2. The Superconducting Wire.

The wire consisted of approximately two pounds of Nb_3Zr manufactured by the Wah Chang Corporation of Albany, Oregon. The wire was cold worked, with an area reduction of 95%, to an outside diameter of 0.010 inches. The outside diameter with enamel insulation varies from 0.011 to 0.012 inches.

The wire was found to have a thermal expansion ratio of $\Delta L/L = 186 \pm 10 \times 10^{-5}$ between 4.2°K and 300°K (See Appendix III).

Boom and Livingston /1/ have published a graph (Figure 1) of the maximum critical current vs. magnetic field for short specimens of the wire. Our original design was based on this curve. However, we find this curve does not apply when the wire is in its own magnetic field. Sections 6 and 7 discuss this further.

The wire behaves much like spring steel, both in strength and elasticity. A sharp kink will severly weaken the wire and is apt to produce a break.

We inadvertantly annealed a short piece (about three inches) with a current of about one ampere at room temperature. The annealed wire behaves much like copper in both strength and elasticity.

3. Coil Number One.

The original plans for the solenoid were based on the Boom and Livingston /1/ curve (Figure 1). However, in order to better evaluate such a solenoid, we decided to construct a preliminary test coil to the same dimensions as required for the final magnet. It was decided to wind it bifilar with respect to the superconducting wire, with taps at the ends of each layer to permit greater flexibility in the investigations. The possibility of a burnout within the windings when the current was suddenly quenched was considered. As a means of protection, each layer of superconducting wire was accompanied by a layer of #47 AWG copper. In principle, with the copper wire wound in with the superconductor, the mutual inductance between the two would be unity. When the superconductor quenches, the induced EMF in the windings due to the collapsing field will be much less with the copper shunt in place than with the superconductor alone, because the current

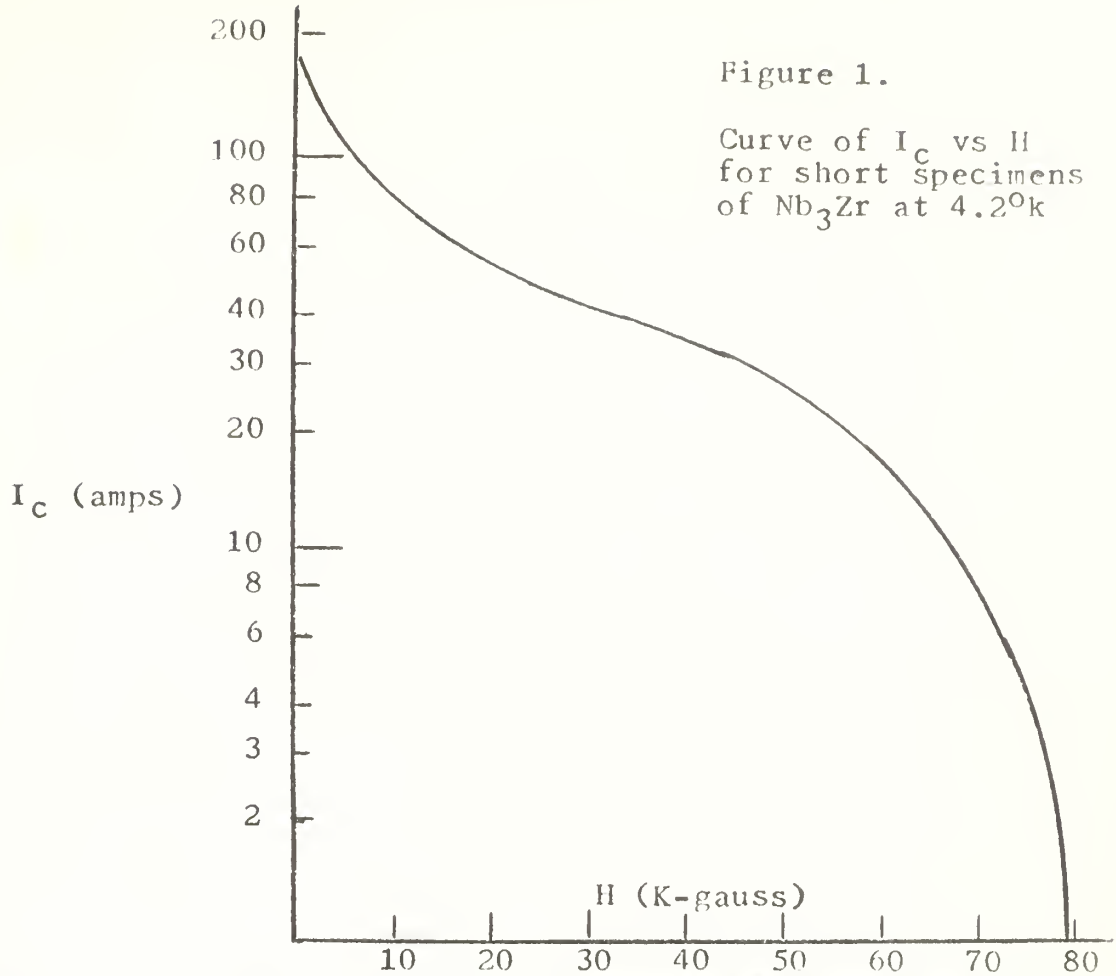

Figure 1.

Curve of I_c vs H for short specimens of Nb_3Zr at 4.2°k

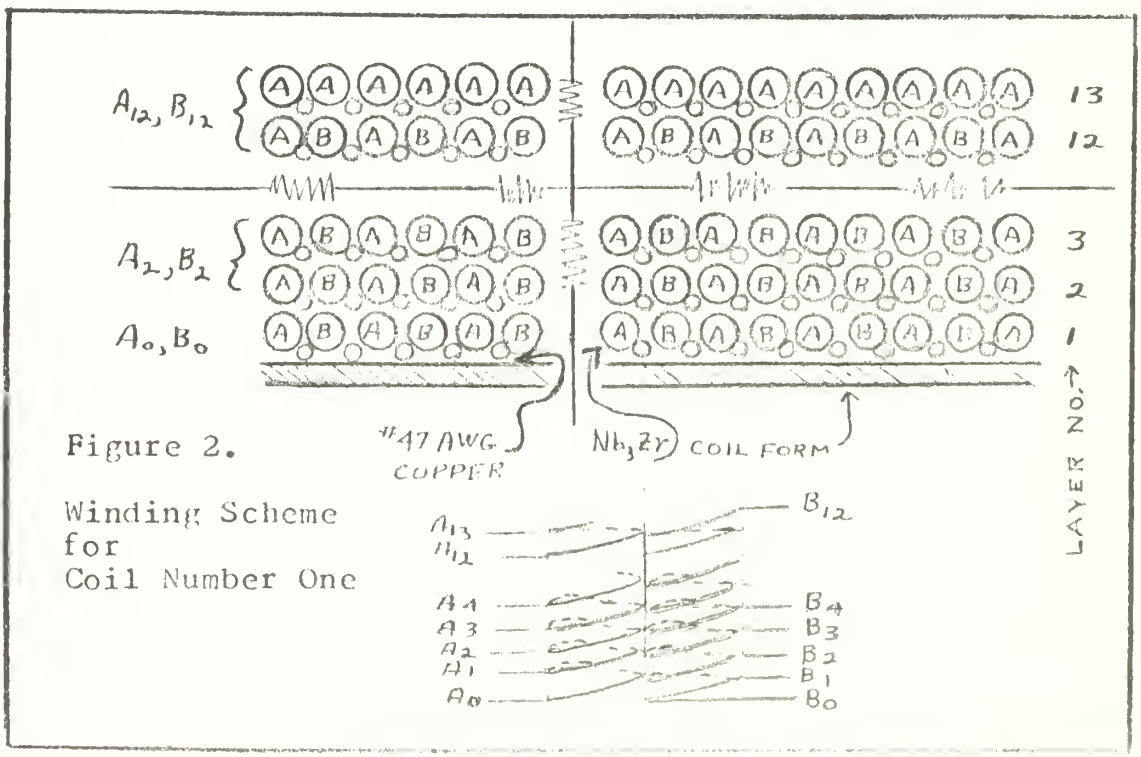

Figure 2.

Winding Scheme for Coil Number One

will tend to shift from the superconductor to the copper and thereby slow the decay of the field. With the 0.010 inch superconductor, we estimated that with careful winding the copper could be made to lie in between the strands of superconductor, without significantly increasing the volume of the windings.

A crude winding device was fabricated, consisting of a variable speed motor, a speed reducer, and a foot rheostat. The coil form was mounted on a protruding shaft. A slide carriage was incorporated and on it were TEFLON washers, for wire tension adjustment, and a wire guide made of a piece of plastic with holes, mounted at such an angle that the four wires would converge at the coil. The tension and positioning of the wires was controlled by hand.

The coil form is 3.475 inches long (inside clearance), 3.900 inches outside diameter of the flange, 3.070 outside diameter of the cylinder, and 3.007 inches inside diameter of the cylinder. The form is constructed of aluminum and insulated with ARMSTRONG C-7 epoxy. Each layer of windings was double wrapped with 0.001 inch MYLAR film. Table 1 lists the number of turns in each layer.

Figure 2 shows schematically the wiring of the coil. Figure 3 is a photograph of the coil and Figure 4 shows the coil mounted for testing.

It was found that the #47 AWG copper wire was too small for two reasons: first, its fragility rendered working with it impractical, and second, it was observed to have burned out when quenched at a high current. Specifically, when loops B1 and B2 were quenched individually at 100 amperes, the copper shunts for these loops burned out internally. The superconductor, however, was not damaged.

It should be noted that we made one trial in a section of the coil that

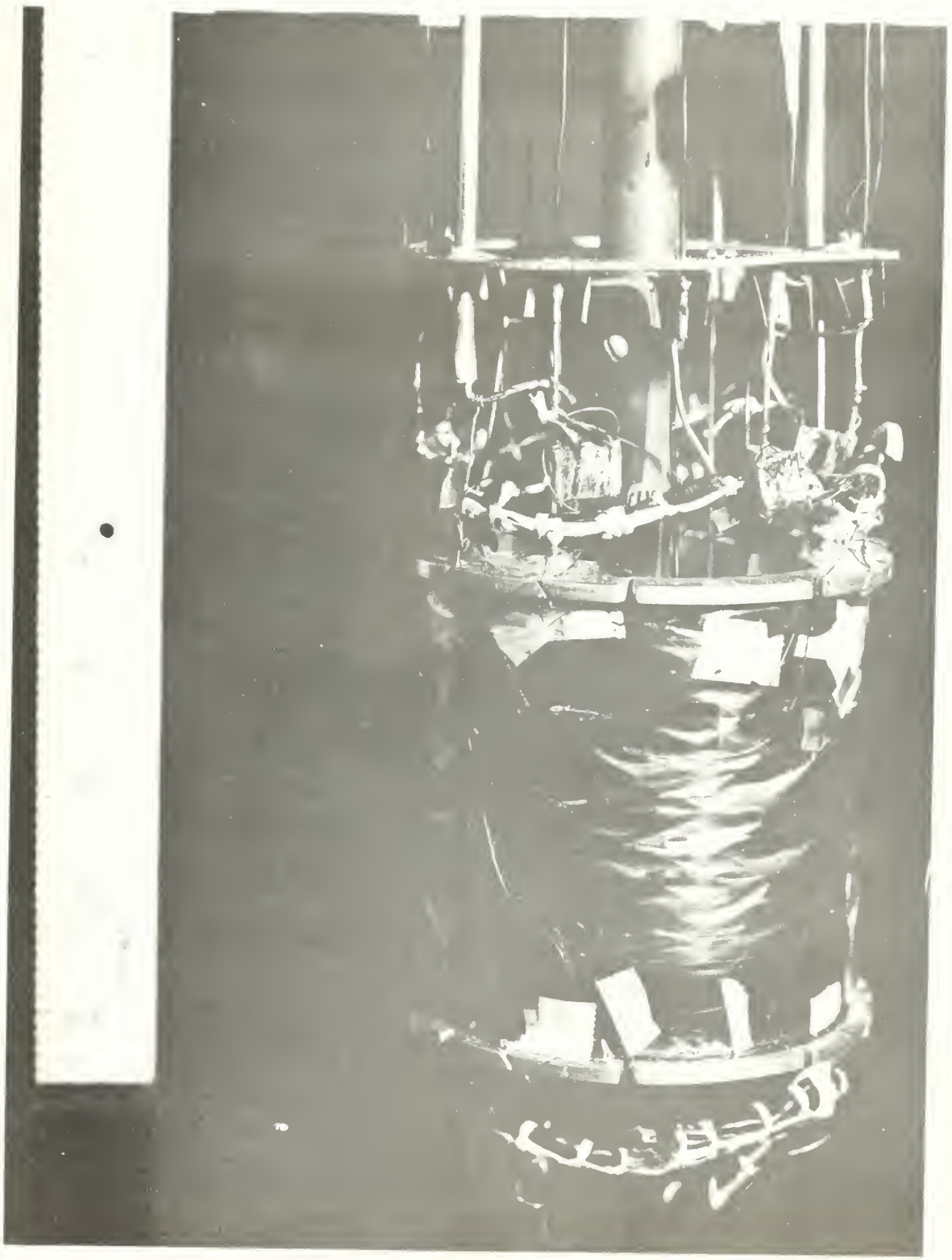

Figure 3. Coil Number One

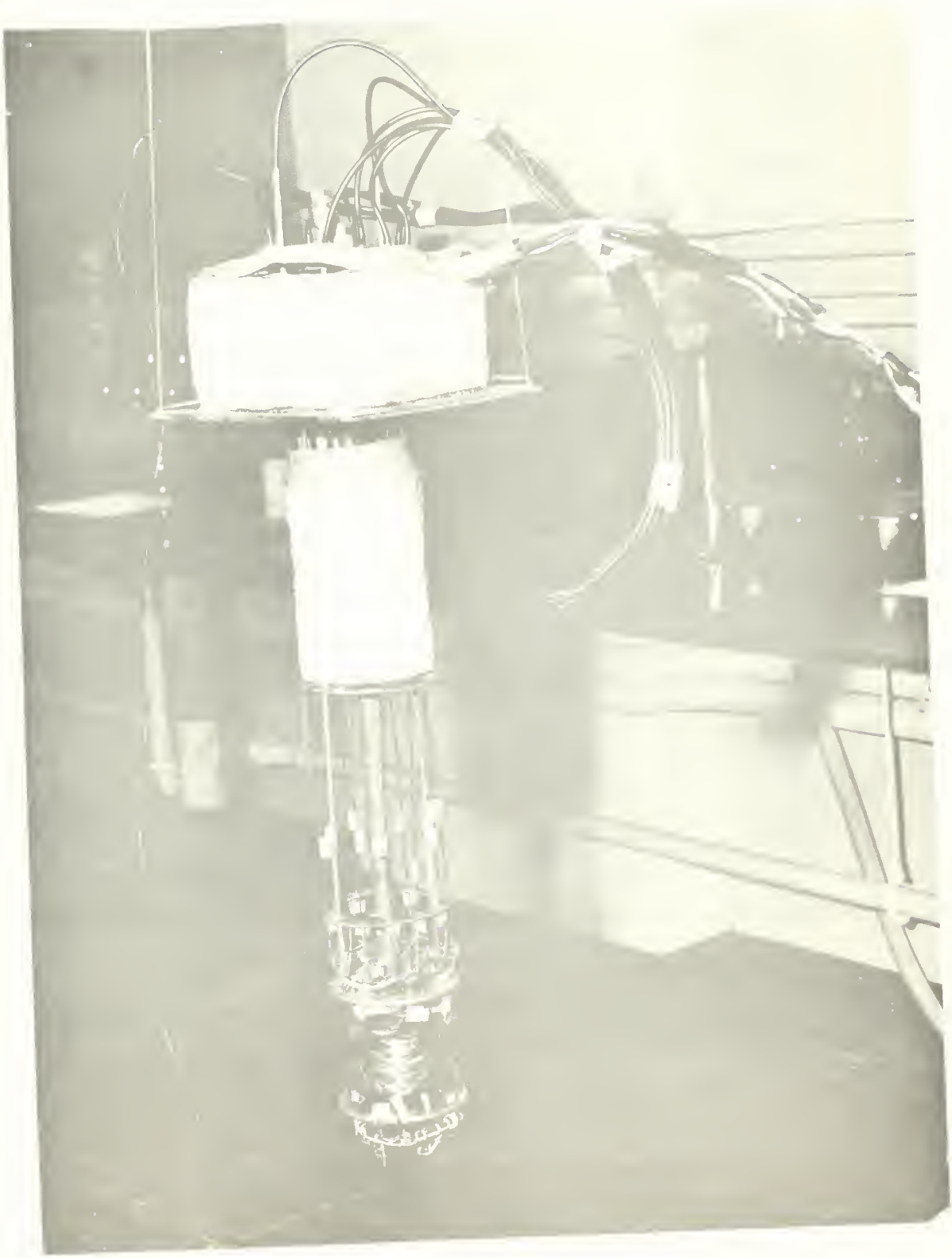

Figure 4. Coil Number One Mounted for Testing

TABLE 1

Turn count and Dimensions of Coil Number One.

Layer Number	Number of "A" Turns	Number of "B" Turns	Est. O.D. of Layer (in.)
1	145	145	3.098
2	152	152	3.127
3	151	151	3.155
4	166	166	3.184
5	156	156	3.212
6	158	158	3.240
7	164	164	3.269
8	164	164	3.297
9	154	154	3.326
10	155	155	3.354
11	161	161	3.382
12	157	157	3.411
13	327	---	3.439
Totals	2210	1883	

had its copper shunt broken. The particular run was with the "A" and "B" loops in series. The loop A7 developed a burnout in the Nb_3Zr wire. The wire appeared to have overheated and melted at the point of burnout, rather than to have shorted to another lead. This illustrates the advantage of the copper shunt wires.

Several of the copper shunts were broken externally in handling. It appears, however, that the #47 AWG may be adequate as a shunt for currents up to 50 amperes.

Three data runs were made on coil number one. On the first run, clamp type connectors were employed at the ends and at the taps between the layers. On the subsequent two runs soldered connectors were used. Appendix II discusses these connectors in detail.

4. Coil Number Two.

The second coil was wound on the same winding device using the same superconducting wire, coil form, and techniques as those used for coil number one with the following exceptions:

a. #30 AWG vice #47 AWG (used on coil number one) copper wire was used as a shunt.

b. The only taps for coil number two were those that involved taps A1, B1, B4, A7, and A11 of coil number one. These were locations of breaks in the Nb_3Zr wire and it was decided best to make the splices externally to the coil. No copper shunts were brought out except at the ends.

c. Clear GLYPTAL was brushed on the windings near the ends of each layer.

d. A three layer lead holder consisting of three fiber rings was attached to the top of the coil form.

The second coil was also wound bifilar with "A" and "B" windings. Table 2 lists the number of turns in each layer. The solder type connections (See Appendix II) were used for connecting to the superconducting wire and for making splices.

A ring assembly was fabricated (Figure 5) for holding the end leads as well as the splices. Sufficient extra wire was left in these rings to allow for making new or different connections in the event of breakage or the development of better connector techniques.

A data run was made on the second coil, and this data is incorporated with that of the first coil (See Section 6.)

The coil may be operated with the "A" and "B" loops in parallel or in series. Some danger exists in series operation in that if a copper shunt should be broken and the coil were to quench, the voltage developed between adjacent windings within the magnet might be sufficient to puncture the insulation, causing an internal burnout or short. Breaks in the copper shunt can be detected by making periodic resistance checks on the coil while it is not superconducting.

From the data we predict that the coil can be operated in series or in parallel with a D.C. current of up to 20 amperes, producing a maximum field within the windings of 9.02 K-gauss. This current will produce a field of 8.0 K-gauss at the center of the solenoid and a mean field within the working volume of the solenoid of about 7.6 K-gauss. It is conceivable that the coil could be "trained" to accept higher currents. This training effect is described in sections 6 and 7.

TABLE 2

Turn Count and Dimensions of Coil Number Two

Layer Number	Number of "A" Turns	Number of "B" Turns	Est. O. D. of Layer (in.)
1	90.0	90.0	3.098
2	83.0	83.0	3.125
3	92.3	92.3	3.153
4	77.6	77.6	3.180
5	81.8	81.8	3.208
6	78.8	78.8	3.236
7	73.2	73.2	3.263
8	82.0	82.0	3.291
9	67.6	67.6	3.318
10	75.5	75.5	3.346
11	82.0	82.0	3.374
12	73.5	73.5	3.401
13	66.4	66.4	3.429
14	73.1	73.1	3.457
15	106.9	106.9	3.484
16	77.1	77.1	3.512
17	96.4	96.4	3.539
18	84.5	84.5	3.567
19	92.6	92.6	3.594
20	78.0	78.0	3.622
21	87.0	87.0	3.650
22	69.1	69.1	3.677
22.5	38.9	38.9	- ---
23	79.2	-- -	3.705
24	143.1	-- -	3.732
25	80.0	-- -	3.760
Totals	2130	1827	

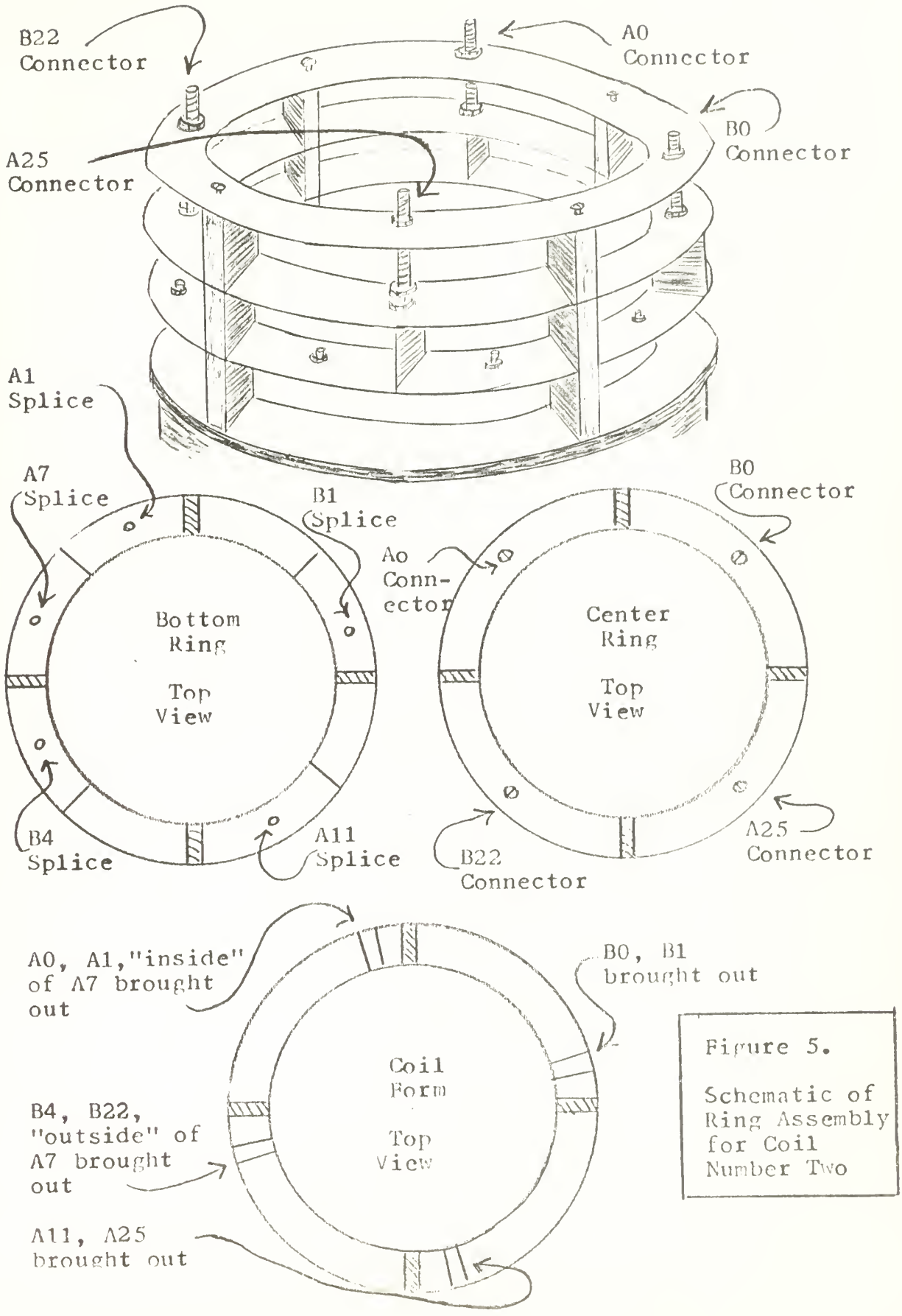

Figure 5.

Schematic of Ring Assembly for Coil Number Two

5. Experimental Techniques

For taking data on the magnets a simple patch panel was fabricated. Figure 6 shows this arrangement schematically. A Superior Electric Company "VERICELL" power supply Type V4050-3 was used. It employs a three phase, 240 volt input into a gang of three variable transformers. Silicon diode rectifiers are delta connected across the transformers. The D. C. output is rated at 50 amperes continuous at zero voltage. We have operated it for periods of less than one minute at currents up to 100 amperes. The D. C. output has a 360 cycle ripple of 4.2% on a non-inductive load.

During the first run a 0-50 ampere meter was used on the "A" side of the patch panel (See Figure 6). Figure 7 shows the modifications made for the data run on the second coil. It involved placing the meters directly on the leads to the magnet. It should be noted that provision was made for the use of batteries on the "B" side; however, batteries were not used. A flux meter for crude measurements of fields within the coil was fabricated (See Appendix V). This meter was employed during the data run on the second magnet.

6. Measurements made on the Coils.

The data taken on coil number one is listed in Table 3, which is arranged so as to show any possible instances of connector limitations on the current. This table does not list data taken when the helium level was believed to be low. For academic reasons only, these data are listed in Table 7. Table 4 is a listing of the data reduction for coil number one. This table omits data believed to have been influenced by connector limitations. Table 5 lists the data and data reductions made on coil number two.

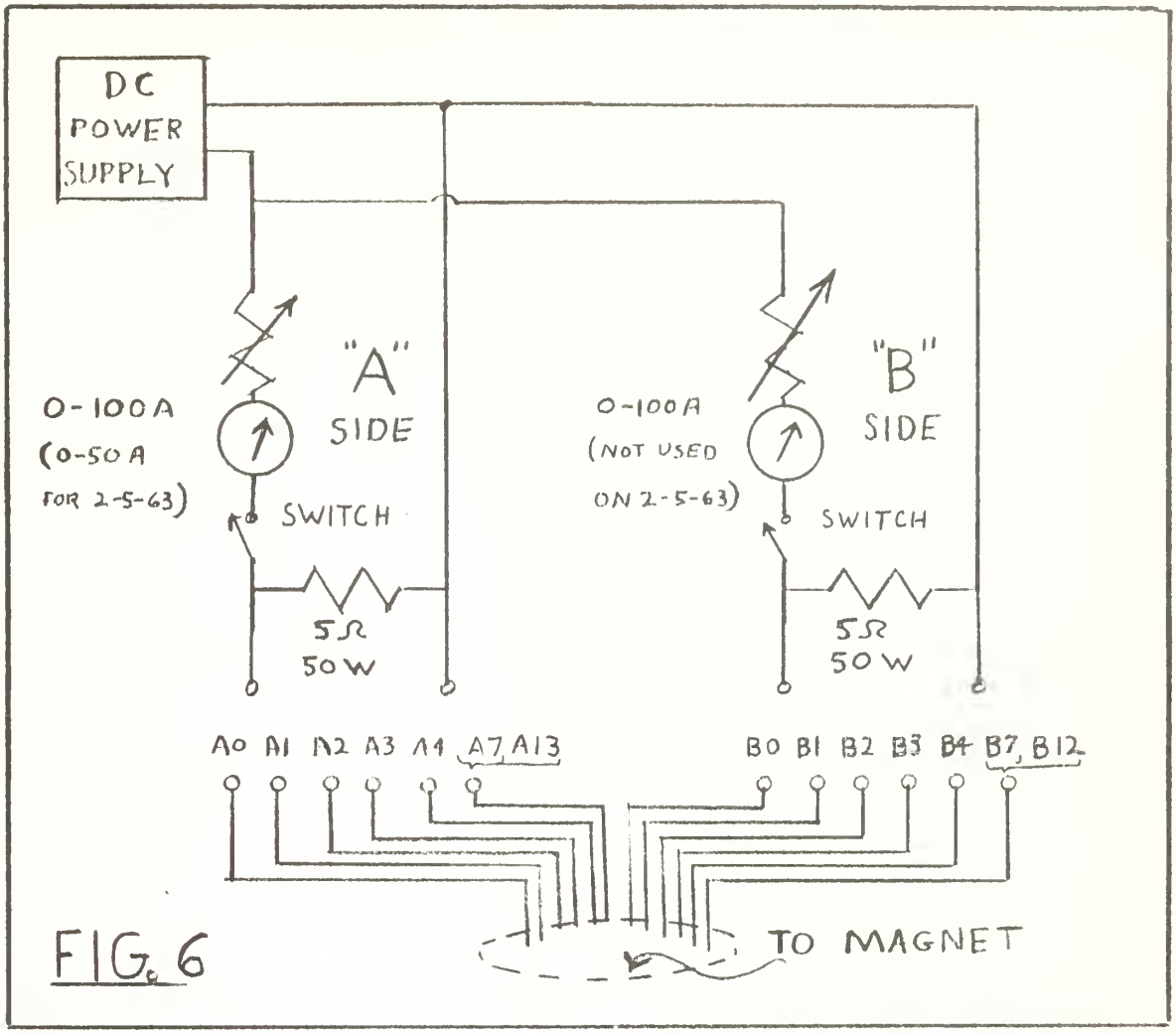
DC
POWER
SUPPLY
"A"
SIDE
0-100A
(0-50A
FOR 2-5-63)
SWITCH
5Ω
50W
"B"
SIDE
0-100A
(NOT USED
ON 2-5-63)
SWITCH
5Ω
50W
A0 A1 A2 A3 A4 A7 A13
B0 B1 B2 B3 B4 B7 B12
TO MAGNET

FIG. 6

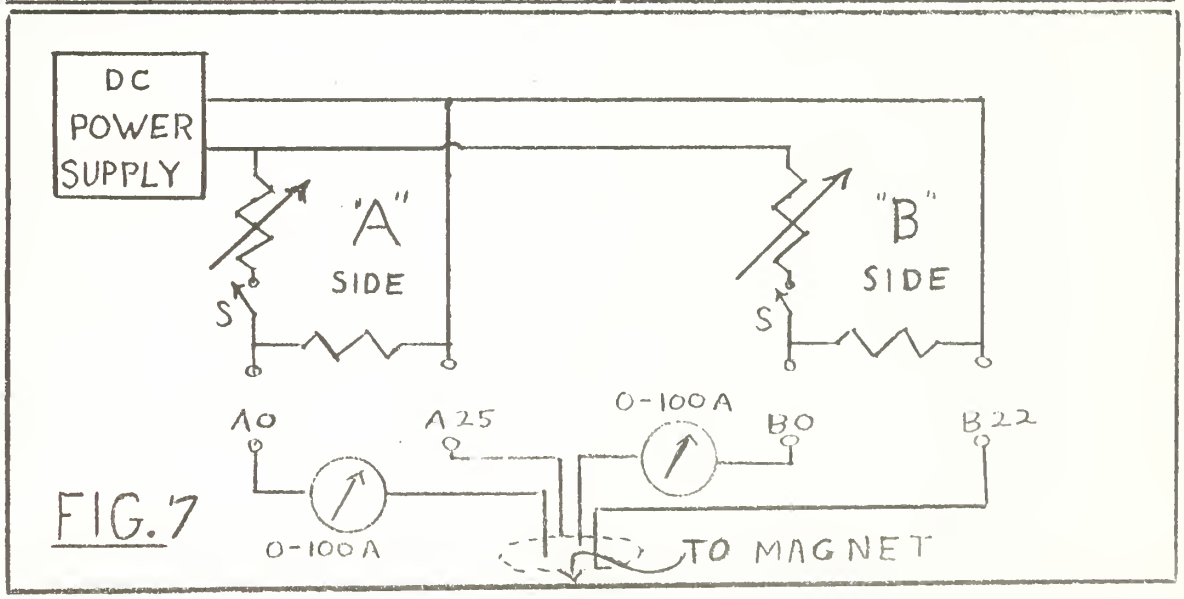
DC
POWER
SUPPLY
"A"
SIDE
S
"B"
SIDE
S
A0
A25
0-100A
B0
B22
0-100A
TO MAGNET

FIG. 7

The flux meter readings used with this coil are evaluated in Table 6. This table does not contain data on quenching. The agreement between calculated fields and measured fields is within 10%, which is within the accuracy of the flux meter.

The fields listed are what we believe to be the maximum fields within the windings. The techniques employed in computing the fields are shown in Appendix IV. Figure 8 shows the quenching currents vs. computed fields for all the data. No attempt is made to draw a curve through these points, however, Figure 9 is a plot of the maximum current vs. maximum field within the windings, for various loops and combinations. This graph is simply the "best" points from Figure 8.

Based on the points of Figure 9, an attempt has been made to correlate our "best" data with the work reported by Montgomery /2/, who states that the maximum current density within the coil can be expressed as

$$j_{max} = j_c/(1+a_1 F/F')$$

Where j_c is the critical current density established by Boom and Livingston /1/, F is a function of α and β, where α is the outside radius of the windings divided by the inside radius and β is the half length of the solenoid divided by the inside radius. The term a_1 is the inside radius of the windings. F' is an empirical function of α and β that (according to Montgomery) describes the induced eddy currents within the wire. The function $F(\alpha, \beta)$ is equivalent to $G\sqrt{\nu}$ used by Boom and Livingston /1/, and is used in computing the fields produced by the coils (See Appendix IV).

From the points of Figure 9 a value of $F'(\alpha, \beta)$ was computed. These are listed in Table 8. A plot of these points of $F'(\alpha, \beta)$ vs.

α is shown on Figure 10. It should be noted that we had packing densities of 0.504, 0.252, 0.249, and 0.135 for the different combinations. The value of packing density used in the report by Montgomery /2/ was 0.48. For the selected points used, we seem to be in agreement with Montgomery; however, the model proposed by Montgomery does not explain the quenching currents observed when we used opposing currents, which produced a net field which was virtually zero.

Figure 11 is a plot of the quenching current vs. field produced by the turns of a respective loop. For example, if loops A1-A4 only were in use, I is plotted against the total field within the magnet; however, if A1-A4 was in series with B1-B4, the value of field plotted is that produced only by the "A" loops or the "B" loops. In this case the total field would be the sum of the fields produced by the separate loops. The purpose of this plot is to illustrate that when the current in "A" is opposed to that in "B", quenching occurs at about the same current as when they are aiding. For example, the fields plotted for the "A" loops is as if "B" were not in use, and the fields plotted for the "B" loops are those that would be produced if "A" were not in use. The sign of the fields has been ignored. We consider this of interest, for in effect it appears that the quenching current is not simply a function of the environmental magnetic field of the wire. The theory proposed by Montgomery, however, assumes that it is. This effect is illustrated here only for the A1-A4 and the B1-B4 loops, on which we have considerable data. However, the same effect is seen in the second coil where parallel aiding and parallel opposing currents were used.

Figure 12 shows two cases of possible training of the coil. It has been observed that when the coil is brought up to the quenching current several times in succession, the quenching current sometimes increases. This effect is not explained.

TABLE 3

Data Taken on Coil Number One (Amperes) Data Taken 2-5-63

Run. No.	Connector Used A0	A1	A2	A3	A4	A13	B0	B1	B2	B3	B4	B12	Remarks*
1	35	(35)											C.L.
2	50+		50+										
3	34	(34)											C.L.
4			18	18									??
5							50+	50+					
6								45	45				
7								38	38				
8							20----------					----20	
9							26----------					----26	
10							30----------					----30	
11							25----------					----25	
12	33----------			----33									
13	33----------			----33									
14	24----------			----24			24----------					----24	S.A.

TABLE 3 (Continued)

Run No.	Connectors used A0	A1	A2	A3	A4	A13	B0	B1	B2	B3	B4	B12	Remarks*
15	26					26	26					26	S.O., refill
16	23					23	23					23	S.A.
17	18					18	18					18	S.A.
18							22					22	
19							22					22	
20	22					22							
21	38					38	38					38	S.O.
22	42					42	42					42	S.O.
23	18					18	18					18	S.A.
24	0					0	0					0	S.A., burnout
25	30+	(30+)											C.L.
26	34+	(34+)											C.L.
27			20	20									??
28	38				38								
29							50+	50+					

TABLE 3 (Continued)

Run No.	Connectors used												Remarks*
	AO	A1	A2	A3	A4	A13	BO	B1	B2	B3	B4	B12	
30							42		24				
31							50+			50+			
32							22				22		
33							26				26		
34									18		18		??
35									21		21		??
36			32		32								??
37			33		33								??
38		(33)			33								C.L.
39		(35)			35								C.L.
40	34				34								
41	36	(36)											C.L.
42	37				37								
43	21				21		21				21		S.O.

TABLE 3 (Continued)

Run No.	Connector Number A0	A1	A2	A3	A4	A13	B0	B1	B2	B3	B4	B12	Remarks*
44	26----------				----------26		-26----------				---------- -26		S.O.
45	23----------				----------23		23----------				----------23		S.A.

Data Taken 4-1-63

Run No.	Connector Number A0	A1	A2	A3	A4	A7	B0	B1	B2	B3	B4	B7	Remarks*
1	53	53							53	53			S.A.
2			53	53			53	53					S.A.
3			40--------		----------40				40--------		----------40		S.A.
4	53	53						53	53				S.A.
5	50	50					50	50					S.A.
6		34----------			----------34			34----------			----------34		S.A.
7		28----------			----------28								
8								28----------				----------28	
9								26----------				----------26	
10		37----------			----------37			-37----------			---------- -37		See note #1
11		37----------			----------37			-24----------			---------- -24		See note #1

TABLE 3 (Continued)

Run No.	A0	A1	A2	A3	A4	A7	B0	B1	B2	B3	B4	B7	Remarks*
12		20----------				----------20		-20----------				---------- -20	See note #2
13		20----------				----------20		22----------				----------22	See note #2
						Data Taken 4-8-63							
1	50	50											
2	52	52											
3		63	63										
4			60	60									
5				68	68								
6	52--------		52										
7	34----------		34										
8	30----------				30								
9	24----------					----------24							
10							(38)	38					C.L.
11								100	100				

TABLE 3 (Continued)

Run No.	A0	A1	A2	A3	A4	A7	B0	B1	B2	B3	B4	B7	Remarks*
12									100+	100+			
13		33----------			33								??
14								56----------				56	??, refill
15								24----------				24	
16								27----------				27	
17		26----------				26							
18	42	42											
19		44	44						44	44			S.A.
20		26	26						26	(26)			C.L.
21				60	60			60	60				S.A.
22									26	(26)			C.L.
23									52--------			52	

*C.L. = Connector limited; S.A. = Series Aiding; S.O. = Series Opposing
?? = See No Reason for apparent discrepancy refill = Refill with He.

TABLE 3 (Continued)

Note #1 : On this run "A" and "B" were brought up together with opposing currents. "A" was held at 37 amperes while the current in "B" was dropped. Both quenched when "B" reached -24 amperes.

Note #2 : On this run "A" and "B" were brought up together with opposing currents. "A" was held at 20 amperes while "B" was brought down to zero and back up to 22 amperes, where both quenched.

TABLE 4
Data Reduction on Coil Number One

Run No.	Loops in Use	I amps	H/I	H K-g	H for Run	Remarks*
				Data Taken 2-5-63		
2	A1-A2	50+	0.0356	1.780		
4	A3	18	0.0181	0.326		??
5	B1	50+	0.0174	0.872+		
6	B2	45	0.0182	0.819		
7	B2	38	0.0182	0.691		
8	B1-B4	20	0.0733	1.468		
9	B1-B4	26	0.0733	1.906		
10	B1-B4	30	0.0733	2.200		
11	B1-B4	25	0.0733	1.831		
12	A1-A3	33	0.0536	1.770		
13	A1-A3	33	0.0536	1.770		
14	A1-A3	24	0.0536	1.287		
	B1-B4	24	0.0733	1.760	3.047	S.A.
15	A1-A3	26	0.0536	1.448		
	B1-B4	-26	0.0733	-1.906	-0.458	S.O.
16	A1-A3	23	0.0536	1.232		
	B1-B4	23	0.0733	1.687	2.919	S.A.
17	A1-A3	18	0.0536	0.965		
	B1-B3	18	0.0536	0.965	1.930	S.A.
18	B1-B12	22	0.2217	4.870		
19	B1-B12	22	0.2270	4.870		
20	A1-A13	22	0.2607	5.740		
21	A1-A13	38	0.2607	9.910		
	B1-B12	-38	0.2217	-8.410	1.500	S.O.
22	A1-A13	42	0.2607	10.95		
	B1-B12	-42	0.2217	-9.30	1.65	S.O.

TABLE 4 (Continued)

Run No.	Loops in Use	I amps	H/I	H K-g	H for Run	Remarks*
23	A1-A13	18	0.2607	4.70		
	B1-B12	18	0.2217	3.98	8.68	S.A.
27	A3	20	0.0181	0.362		??
28	A1-A4	38	0.0733	2.710		
29	B1	50+	0.0174	0.872+		
30	B1-B2	42	0.0356	1.495		
31	B1-B3	50+	0.0536	2.680+		
32	B1-B4	22	0.0733	1.613		
33	B1-B4	26	0.0733	1.906		
34	B3-B4	18	0.0389	0.700		??
35	B3-B4	21	0.0389	0.817		??
36	A3-A4	32	0.0389	1.245		
37	A3-A4	33	0.0389	1.285		
40	A1-A4	40	0.0733	2.935		
42	A1-A4	37	0.0733	2.715		
43	A1-A4	21	0.0733	1.540		
	B1-B4	-21	0.0733	-1.540	0	S.O.
44	A1-A4	26	0.0733	1.906		
	B1-B4	-26	0.0733	-1.906	0	S.O.
45	A1-A4	23	0.0733	1.689		
	B1-B4	23	0.0733	1.689	3.378	S.A.
				Data Taken 4-1-63		
1	A1	53	0.0174	0.924		
	B3	53	0.0181	0.969	1.884	S.A.
2	A3	53	0.0181	0.960		
	B1	53	0.0174	0.924	1.884	S.A.

TABLE 4 (Continued)

Run No.	Loops in Use	I amps	H/I	H K-g	H for Run	Remarks*
3	A3-A4	40	0.0389	1.555		
	B3-B4	40	0.0389	1.555	3.110	S.A.
4	A1	53	0.0174	0.924		
	B2	53	0.0182	0.975	1.899	S.A.
5	A1	50	0.0174	0.872		
	B1	50	0.0174	0.872	1.744	S.A.
6	A2-A4	34	0.0560	1.905		
	B2-B4	34	0.0560	1.905	3.810	S.A.
7	A2-A7	28	0.1124	3.150		
8	B2-B7	28	0.1124	3.150		
9	B2-B7	26	0.1124	2.965		
10	A2-A7	37	0.1124	4.160		
	B2-B7	-37	0.1124	-4.160	0	See Note #1
11	A2-A7	37	0.1124	4.160		
	B2-B7	-24	0.1124	-2.700	1.46	See Note #1
12	A2-A7	20	0.1124	2.150		
	B2-B7	-20	0.1124	-2.250	0	See Note #2
13	A2-A7	20	0.1124	2.150		
	B2-B7	22	0.1124	2.479	4.729	See Note #2
				Data Taken 4-8-63		
1	A1	50	0.0174	0.872		
2	A1	52	0.0174	0.906		
3	A2	63	0.0182	1.145		
4	A3	60	0.0181	1.085		
5	A4	68	0.0199	1.352		
6	A1-A2	52	0.0356	1.850		
7	A1-A3	34	0.0536	1.820		

TABLE 4 (Continued)

Run No.	Loops in Use	I amps	H/I	H K-g	H for Run	Remarks*
8	A1-A4	30	0.0733	2.200		
9	A1-A7	24	0.1300	3.120		
11	B2	100	0.0182	1.820		
12	B3	100+	0.0181	1.810+		
13	A2-A4	33	0.0560	1.850		
14	B2-B7	56	0.1124	6.300		See Note #3
15	B2-B7	24	0.1124	2.700		
16	B2-B7	27	0.1124	3.040		
17	A2-A7	26	0.1124	2.940		
18	A1	42	0.0174	0.732		
19	A2	44	0.0182	0.800		
	B3	44	0.0181	0.796	1.596	S.A.
21	A4	60	0.0199	1.195		
	B2	60	0.0182	1.090	2.285	S.A.
23	B3-B4	52	0.0389	2.022		

*For notation used in the remarks column and for notes #1 and #2, see Table 3.

Note #3: It is believed an error may have been made in recording this data point.

TABLE 5

Data and Data Reduction on Coil Number Two

Data Taken 4-25-63

Run No.	Loops in Use	I amps	H K-g	H for Run	Remarks*
1	A	15	3.64		
2	B	23	4.80		
3	A	13.2	3.21		
	B	14	2.92	6.13	P.A.
4	A	13.2	3.21		
5	B	21.8	4.54		
6	A	11	2.67		
	B	-20	-4.17	-1.40	P.O.
7	A	20.5	4.97		
	B	21	4.38	9.35	P.A.
8	A	20.5	4.97		
	B	20.5	4.26	9.23	P.A.
9	A	14	3.40		fast rise
	B	14	2.92	6.32	P.A.
10	A	16	3.88		
	B	17.5	3.64	7.52	P.A.
11	A	16.1	3.91		
	B	17.8	3.71	7.62	P.A.
12	A	17.4	4.24		slow rise
	B	19.5	4.07	8.31	P.A.
13	A	15.2			
	B	17			C.R., P.A.
14	A	17.1	4.15		
	B	-19.5	-4.07	0.08	P.O.
15	A	21	5.11		
	B	-21	-4.38	0.73	P.O.

TABLE 5 (Continued)

Run No.	Loops in Use	I amps	H K-g	H for Run	Remarks*
16	A	21	5.11		
	B	-22.5	-4.68	0.53	P.O.
17	A	8.2			
	B	8.0			C.R., P.A.
18	A	10.1			
	B	10.0			C.R., P.A.
19	A	15.3			
	B	17.0			C.R., P.A.
20	A	17.1			
	B	17.0			C.R., P.A.
21	A	19	4.62		
	B	19.1	3.98	8.60	P.A.
22	A	15.8			
	B	-16			C.R., P.O.
23	A	0			
	B	0			C.R.
24	A	22.5	5.47		
25	B	24	5.00		
26	A	24	5.83		

*P.A. = parallel aiding; P.O = parallel opposing
C.R. = calibration run for flux meter (NO QUENCHING)

TABLE 6

Calibration Runs for the Flux Meter using Coil Number Two

Run No.	Loops in use	I amps	H_c * K-g	H_c for Run	H_m **	Remarks ***
13	A	15.2	3.26			
	B	17	3.13	6.39	6.9	P.A.
17	A	8.2	1.76			
	B	8.0	1.47	3.23	3.4	P.A.
18	A	10.1	2.17			
	B	10.0	1.84	4.01	4.3	P.A.
19	A	15.3	3.28			
	B	15.0	2.76	6.04	6.35	P.A.
20	A	17.1	3.67			
	B	17.0	3.13	6.80	7.4	P.A.
22	A	15.8	3.39			
	B	-16	-2.94	0.45	0.35	P.O.

* B_c = calculated field at the center of the solenoid

** B_m = flux meter reading

*** P.A. = parallel aiding; P.O. = parallel opposing

TABLE 7

Data on Coil Number One that was possibly influenced by Low Helium Level

Data Taken 2-5-63				Data Taken 4-1-63			
Run No.	Loops in use	I amps	Remarks	Run No.	Loops in use	I amps	Remarks
14a	A1-A3	18		13a	B2-B4	22	
	B1-B4	18	S.A.	13b	B2-B4	21	
14b	A1-A3	18		23a	A4-A7	0	
	B1-B4	-18	S.O.	23b	A4-A7	10	
14c	A1-A3	17		23c	B4-B7	10	
	B1-B4	-17	S.O.				

TABLE 8

$F'(\alpha, \beta)$ vs. α for various Runs

Date of Run	Run No.	Loops in use	Packing Fraction*		$F'(\alpha, \beta)$
4-8	11	B2	0.252	1.0065	0.00468
4-8	12	B3	0.252	1.0064	0.00466
2-5	31	B1-B3	0.252	1.028	0.00986
4-1	3	A3-A4 B3-B4	0.504	1.0171	0.01604
4-1	6	A2-A4 B2-B4	0.504	1.028	0.0136
4-25	25	B	0.135	1.207	0.0212
4-25	12	A&B	0.249	1.225	0.0468
4-25	21	A&B	0.249	1.225	0.0470
2-5	23	A1-A13 B1-B12	0.504	1.120	0.0535
4-25	8	A&B	0.249	1.225	0.0533
4-25	7	A&B	0.249	1.225	0.0554

*Packing Fraction = cross sectional area of the wire divided by the area of the windings occupied by the wire.

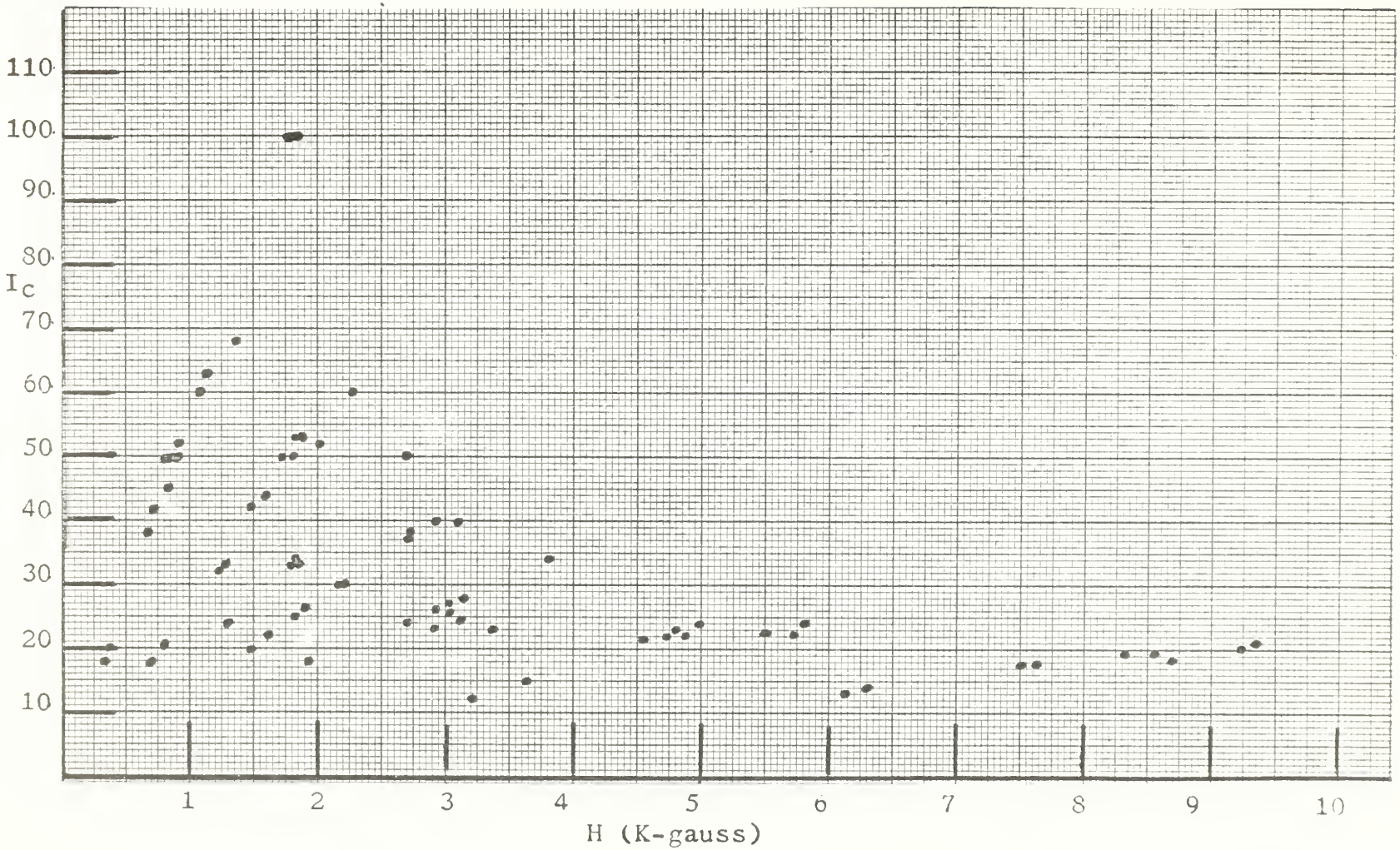

Figure 8. Quenching Current vs Magnetic Field for all the Data

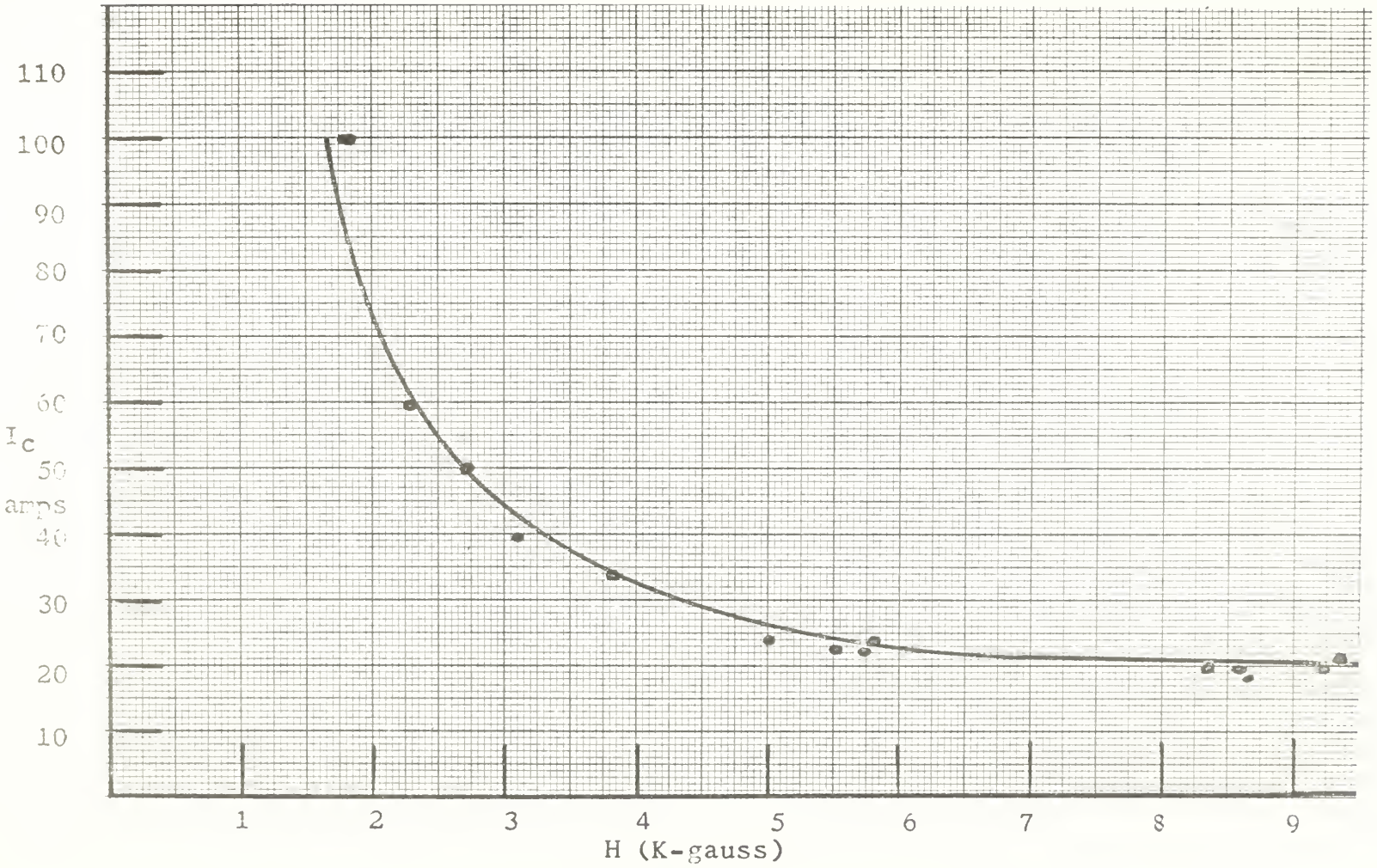

Figure 9.

Plot of I_c vs H for our "Best" Data Points

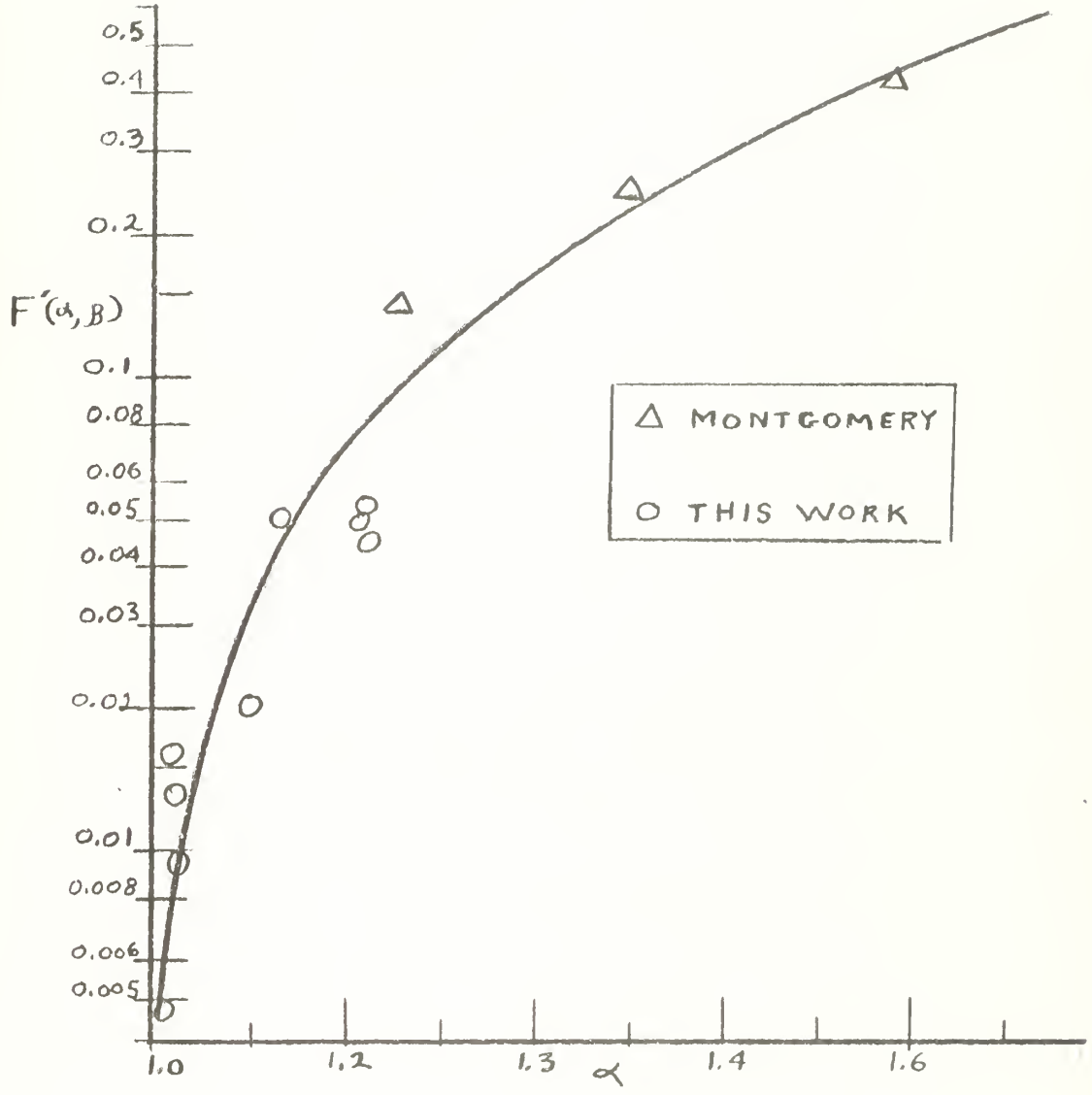

Figure 10.

Plot of $F'(\alpha,\beta)$ vs α

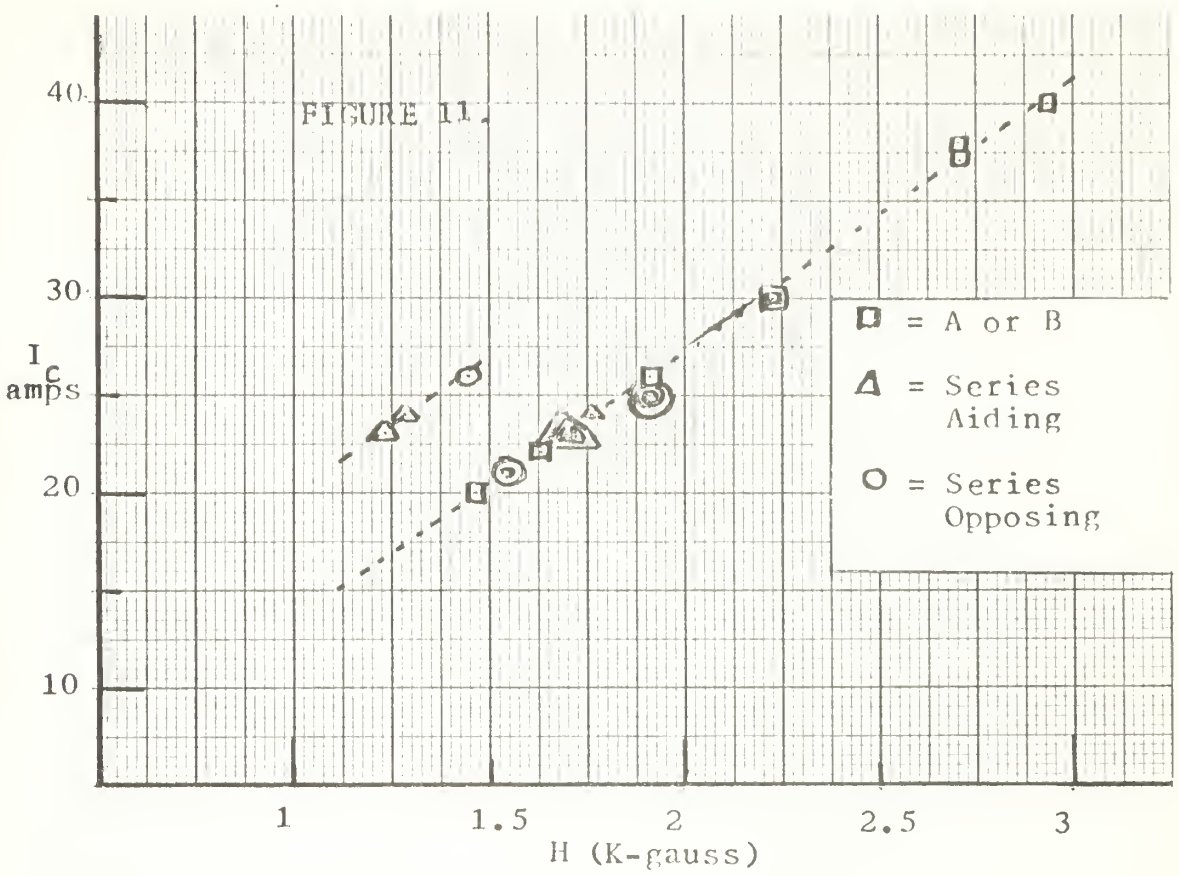

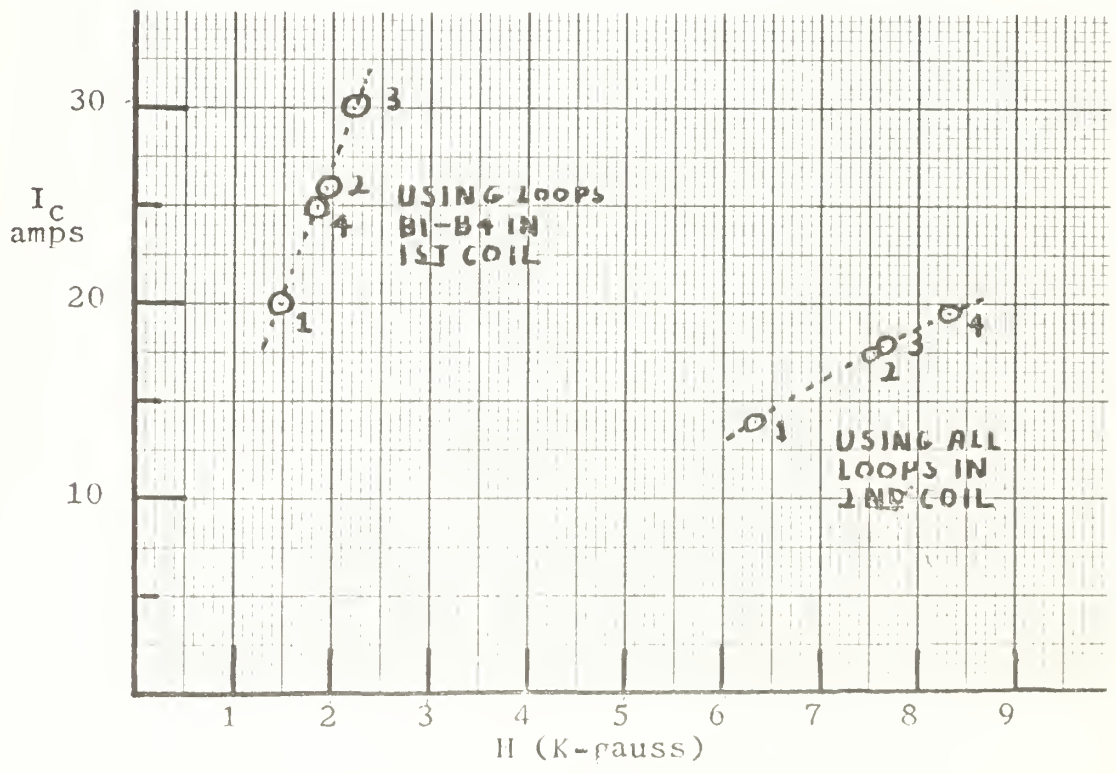

Figure 12. Plot of I_c vs H to show "Training"

7. Conclusions.

The inability of the Nb_3Zr coils to [illegible] magnetic fields comparable to those found by Zoom and [illegible] samples of wire, as well as the inability of the wire [illegible] capability in a sequence of runs is clearly manifested [illegible]

The hypothesis presented by Montgomery appears to apply to our coils only when the currents in the two sets of windings are additive. In the cases when the two currents are opposing, producing a net field of essentially zero, we still observe quenching currents comparable to those obtained when the currents are additive. This appears to discredit the model proposed by Montgomery.

The "training" effect (See Figure 12) appears to be limited to a range of maximum currents vs. field, however, we believe the phenomenon does exist. We propose no mechanism for describing it. It is believed that this effect probably contributed to the wide spread in the data points.

It appears that the rate at which the current is increased in the coil may influence the point at which it quenches. For example, consider runs 9 and 12 on coil number two. On run 9 the current was deliberately increased as fast as possible. The magnet quenched at 14 amperes and 5.32 K-gauss. On run 12 the current was applied very slowly. The quenching current was 19.5 amperes, producing a field of 6.31 K-gauss. There are two other factors that may have influenced this. First, run 9 was in a sequence where "training" had been observed; second, on run 9 the current had been momentarily left on the magnet after quenching, possibly heating the coil and thereby limiting the current in run 9.

The degree to which faulty connectors or a faulty section of the wire

influenced the data cannot be estimated. There exists a possibility that some faulty connector or section of wire, on overheating and consequently heating, undergoes some sort of change resulting in a different behavior on the subsequent run. If this occurred, it could not be detected. Some runs were deliberately omitted from the final data computations where there was substantial evidence that the connectors had somehow limited the behavior of the coil.

APPENDIX I

HIGH CURRENT MAGNET LEADS

The design of any high current superconducting magnet must encompass considerations of the problem of passing high currents into liquid helium. There are two basic opposing effects that must be considered: first, the Ohmic heating of the lead must be kept as low as possible; second, the thermal conduction along the wire or lead must be kept as low as possible. The first problem could be solved simply by using a wire of sufficiently large cross-sectional area; however this would defeat the second problem.

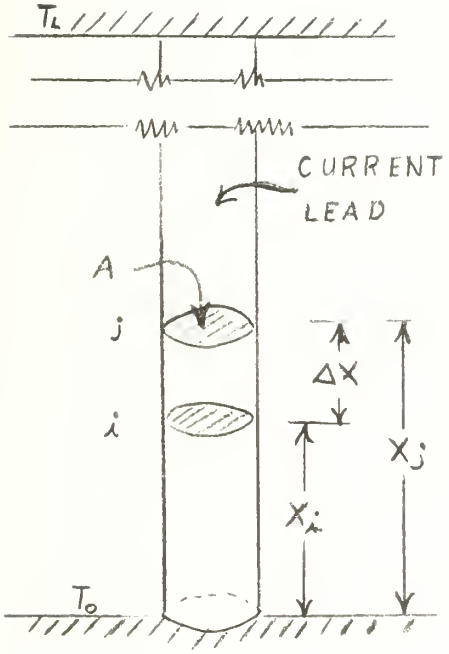

Figure 13

In an analysis of the problem, consider Figure 13. The bottom of the lead is kept at temperature T_o (liquid helium, in our problem), whereas the top is kept at temperature T_L. The lead is assumed to have a uniform cross-sectional area A. Now consider the segment of wire, i-j, located between x_i and x_j. The rate of "heat flow" into this segment (assuming $T_j > T_i$) is $k_j A \partial T_j / \partial x$, where k_j is the thermal conductivity in watts/cm-°K corresponding to T_j. The Ohmic heating in the i-j segment is simply $I^2 \rho \Delta x/A$, where ρ may be considered the resistivity (in ohm-cm) corresponding to the mean temperature of the segment. The rate of "heat flow" out of the segment is $k_i A \partial T_i / \partial x$ plus a term that must allow for gas cooling along the wire. (For our problem we ignore cooling by radiation, since it is at most a second order effect.) The gas cooling term will be proportional to the molar specific

heat of the gas, c_p, the temperature gradient between the gas and the surface of the lead, ΔT, the number of moles of gas per second coming in contact with the lead, n, and the surface area of the segment, $c_w \Delta x$, where c_w is the effective circumference of the lead. Then the gas cooling term would be proportional to $nc_p c_w \Delta T \Delta x$. However, since n and ΔT are functions of the past history of the gas, we can combine them into the constant of proportionality, g, so that the gas cooling term is then $gc_p c_w \Delta x$.

Collecting terms, we get:

$$k_j A \partial T_j / \partial x + I^2 \rho \Delta x / A = k_i A \partial T_i / \partial x + gc_p c_w \Delta x \qquad (1)$$

Rearranging and dividing by Δx, we get:

$$\frac{k_j A \partial T_j / \partial x - k_i A \partial T_i / \partial x}{\Delta x} = -I^2 \rho / A + gc_p c_w \qquad (2)$$

By the sign convention established in Figure 13, and assuming k is approximately constant over Δx, the left side of equation (2) is, by definition, the second derivative;

then

$$\partial^2 T / \partial x^2 = -I^2 \rho (T) / A^2 k(T) + gc_p c_w / Ak(T) \qquad (3)$$

Solutions to equation (3) were attempted using the CDC-1604 computer. The technique assumed no gas cooling. The simplified equation was approached with the central difference method, where a 39 by 39 matrix was programed. The coefficients of the matrix, containing the temperature dependant ρ and k, were obtained from an assumed solution to equation (3). The computer solutions to the matrix were compared to the assumed solutions and iterations were made until reasonable agreement was reached between the two. The technique, although useful, was not entirely successful. Since gas

cooling had been neglected, it was considered more advantageous to experiment with actual leads rather than to refine computer techniques.

An experiment was conducted in which an attempt was made to measure the temperature along various lead wires carrying various currents into liquid helium. The method of temperature measurement was to measure the voltage drop across five centimeter segments of the lead wire. From the voltage drop, a resistivity was computed, and from a resistivity vs. temperature curve, the temperature corresponding to the mean position between the voltage probes was determined.

Our principal aim was to determine temperature vs. distance curves for the various conditions. From these curves it was planned to establish temperature gradients at the helium level and thus determine what size lead wire would be the most efficient for a given current.

Each lead wire had attached to it six voltage probes, spaced five centimeters apart. The voltage probes were #34 AWG, enamel insulated copper wires. They were soldered to the copper current leads and then brought along side the current leads. The assembly consisted of six current leads of sizes #14, #16, #18, #20, #22, & #24 conductor grade copper, with a common #14 AWG copper wire returning from the bottom. The assembly was supported in a STYROFOAM bowl. One sixth inch copper tubing was punched through the STYROFOAM and sealed in place with DEVCON B, an epoxy-steel mixture. It was found that a thin layer of the DEVCON was sufficient to seal the bottom of the bowl for holding liquid nitrogen. The copper current leads were soldered to the bottom of the copper tubing, and the voltage leads were threaded through it. One-eighth inch plastic tubing was placed over the current leads down to about two centimeters from the helium level. This tubing was sealed to the copper tubing with DUCO cement. The purpose of the plastic tubing was to increase the gas cooling effect by concentrating the helium flow

around the leads. Similar tubing was put on the top of the copper tubing and brought down to the side of the cryostat. This allowed for selectively closing the tubes for studying variations with different conditions of gas cooling. The plastic tubing at the top also served as a helium trap to prevent air from being drawn into the cryostat. The voltage leads were brought through the plastic tubing via slits which were then sealed with GLYPTAL. Current to the leads going into helium was supplied via a patch panel and regulated by a carbon pile resistor. The voltage leads were passed through a six pole, six throw wafer switch and then to a two pole, six throw wafer switch and then to a Hewlett-Packard micro-volt meter. Figure 14 is a schematic of this arrangement.

For purposes of data reduction, a synthetic ρ vs T curve was constructed based on values listed in the Chemical Rubber Company Handbook. Figure 15 shows this curve. Data on each lead was normalized to this curve using the resistivity of the probes that were in the helium for the base of the normalization. The normalizing technique was to multiply each value of the computed resistivity by a number that would adjust the values of ρ, for the probes immersed in helium, to a value of 1.00×10^{-3} ohm-cm. Since we had made no calibration runs on each lead to establish a ρ vs T curve for that lead, this was the best we could do with the data. Although it was realized that accurate temperatures were not measured, it was hoped that the relative temperature gradients between the various leads, under the various conditions imposed, could be found with reasonable accuracy.

When the experiment was proposed it was assumed that the temperature gradient near the helium level would be of the order of 1-2 degrees/cm. However we observed that in this region the gradient was only slightly above zero. In fact for most curves the gradients could not be resolved at the

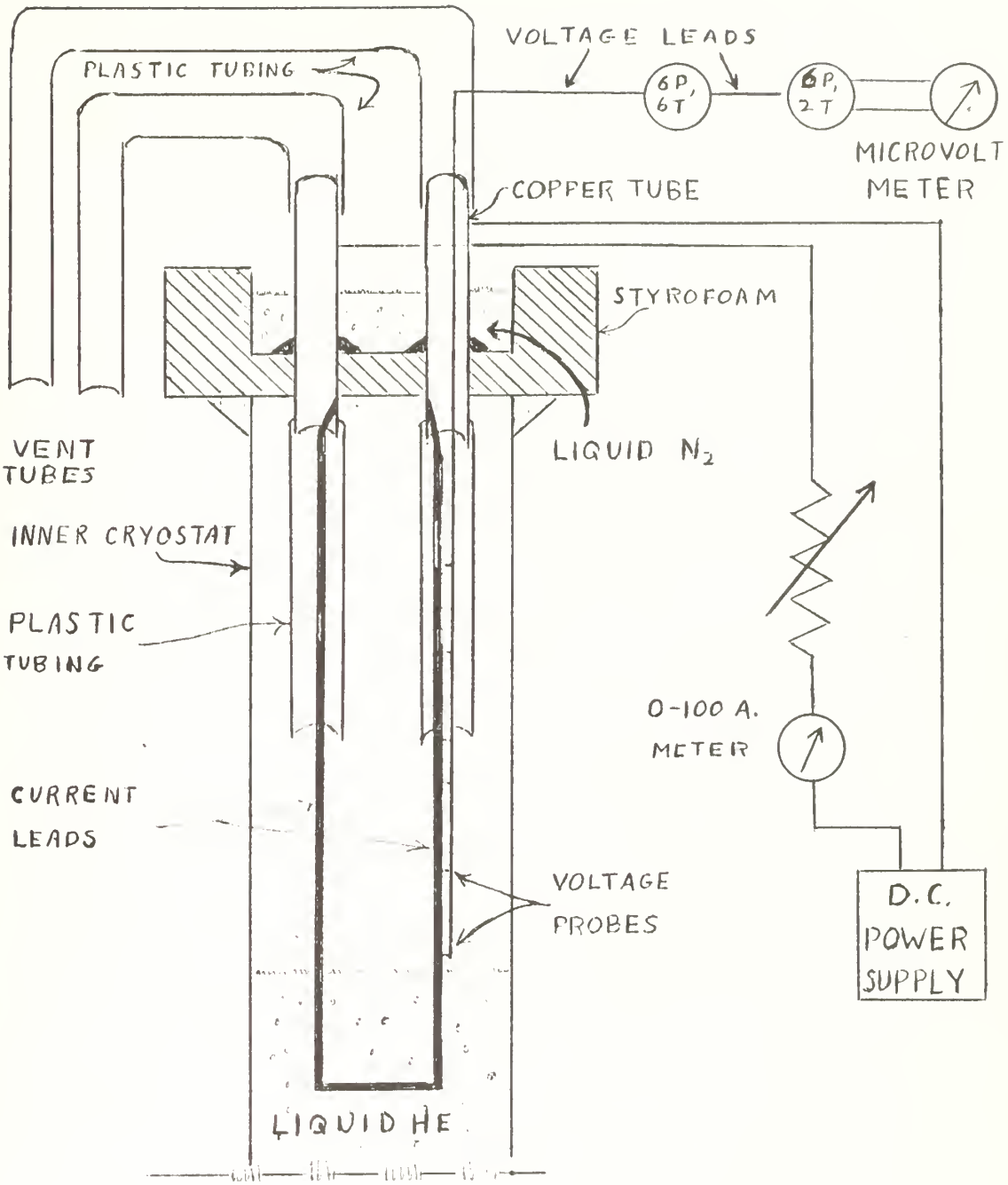

Figure 14.

Schematic of Apparatus used in "Heat Flow" Experiment

liquid helium level. We then decided to establish the gradients at the point where T = 10°K. The values of dT/dx for all curves was determined at T = 10°K, and the values of AdT/dx were plotted against A for each current. From these curves the minimum value of AdT/dx was looked for. In many instances the data did not include currents low enough to establish a minimum exactly. However, the general region of where this minimum would have occurred was assumed and a plot of current vs. optimum wire size was established. (Figure 18)

Table 9 lists the data taken and the values of AdT/dx at 10°K for each run. Figure 16 is a sample of the T vs x curves used for determining the slopes. Figure 17 shows the various AdT/dx vs A curves. From these graphs the optimum wire sizes were inferred. Table 10 lists these values.

A similar experiment was reported by Sobol and McNichol /3/ using currents up to one ampere. Their technique, however, was to determine heat influx by helium boiling rates rather than temperature measurement. They have published values of optimum wire size for 0.5 and 1.0 amperes. These are included in table 10 and plotted on Figure 18.

This experiment was hastily done, because of the large consumption of helium involved, and consequently the results are not as reliable as we had hoped they would be. The resolution of the data was not good enough to construct seperate curves of current vs optimum lead size for each of the four conditions: long wire with and without gas cooling ($L \cong 38$ cm) and short wire ($L \cong 28$ cm), with and without gas cooling. It may be stated, however, that the long wire was more efficient than the short wire. Figure 18 represents what we believe to be a mean between the four conditions.

TABLE 9-a

Data on #14 AWG Wire — Vent tube open

I (amps)	L (cm)	x (cm)	$\rho x 10^{-8}$ (ohm-cm)	T (°K)	$AdT/dx * x 10^{-3}$
10	29.5	16.5	1.58	17.0	
		11.5	1.18	10.0	
		6.5	1.04	6.5	
		1.5	1.04	6.5	
		----	1.00	4.2	20.0
10	35.7	22.7	8.80	49.0	
	17	17.7	2.69	26.5	
		12.7	1.37	14.0	
		7.7	1.06	7.0	
		2.7	1.04	6.5	32.4
20	29.0	16.0	1.47	15.5	
		11.0	1.11	9.5	
		6.0	1.02	4.8	
		1.0	1.00	4.2	
		----	1.00	4.2	24.0
30	28.0	15.0	1.58	17.0	
		10.0	1.03	5.5	
		5.0	1.00	4.2	
		0.0	0.99	4.2	
		----	1.00	4.2	43.6

TABLE 9-a (Continued)

Data on #14 AWG Wire — Vent Tube Open

I (amps)	L (cm)	x (cm)	$\rho \times 10^{-8}$ (ohm-cm)	T (°K)	AdT/dx * x 10^{-3}
30	36.0	23.0	6.89	46.2	
		18.0	2.20	23.0	
		13.0	1.26	13.0	
		8.0	1.04	6.0	
		3.0	0.98	4.2	30.3
40	29.0	16.0	3.91	34.0	
		11.0	2.58	25.8	
		6.0	2.35	24.1	
		1.0	1.08	7.5*	
		----	1.00	4.2	83.5
50	28.7	15.7	2.79	27.0	
		10.7	1.30	13.0	
		5.7	1.18	10.0	
		0.7	1.14	9.3	
		----	1.00	4.2	4.2
50	36.2	23.2	9.56	53.5	
		18.2	2.46	25.0	
		13.2	1.31	13.1	
		8.2	1.11	8.5	
		3.2	1.05	6.5	25.0

TABLE 9-a (Continued)

Data on #14 AWG Wire				Vent Tube Open	
I (amps)	L (cm)	x (cm)	$\rho \times 10^{-8}$ (ohm-cm)	T (°K)	$AdT/dx * \times 10^{-3}$
70	28.5	15.5	1.51	1.61	
		10.5	1.14	9.5	
		5.5	1.03	5.5	
		0.5	1.01	4.8	
		----	1.00	4.2	24.5
70	37.1	24.1	3.32	30.2	
		19.1	2.07	21.7	
		14.1	1.26	12.2	
		9.1	1.07	7.0	
		4.1	1.02	5.5	25.0
				Vent Tube Closed	
10	29.1	16.1	5.35	41.0	
		11.1	1.61	17.5	
		6.1	1.22	11.5	
		1.1	1.22	11.5	
		----	1.00	4.2	??
10	37.5	24.5	10.3	55.5	
		19.5	3.02	28.8	
		14.5	1.44	15.0	
		9.5	1.34	13.5	
		4.5	1.24	11.8	??

TABLE 9-a (Continued)

Data on #14 AWG Wire — Vent Tube Closed

I (amps)	L (cm)	x (cm)	$\rho x 10^{-8}$ (ohm-cm)	T (°K)	$AdT/dx * x 10^{-3}$
30	29.6	16.6	3.53	32.0	
		11.6	1.39	14.5	
		6.6	1.07	7.0	
		1.6	1.02	5.2	
		----	1.00	4.2	34.5
30	37.3	24.3	5.43	41.3	
		19.3	1.86	20.0	
		14.3	1.24	11.8	
		9.3	1.08	7.2	
		4.3	1.05	6.5	26.1
50	28.0	15.0	3.64	32.5	
		10.0	1.49	15.8	
		5.0	1.09	7.8	
		0.0	1.03	5.6	
		----	1.00	4.2	29.2
50	37.4	24.4	5.86	42.6	
		19.4	2.14	22.5	
		14.4	1.30	13.0	
		9.4	1.15	9.8	
		4.4	1.09	7.8	10.4

TABLE 9-a (Continued)

Data on #14 AWG Wire				Vent Tube Closed	
I (amps)	L (cm)	x (cm)	$\rho x 10^{-8}$ (ohm-cm)	T (°K)	AdT/dx * x 10^{-3}
70	28.0	15.0	3.91	34.0	
		10.0	1.55	16.5	
		5.0	1.08	7.5	
		0.0	1.01	5.0	
		-----	1.00	4.2	29.2
70	37.5	24.5	5.90	43.0	
		19.5	1.94	21.0	
		14.5	1.24	12.0	
		9.5	1.10	13.2	
		4.5	1.07	7.0	12.5

TABLE 9-b

Data on #16 AWG Wire				Vent Tube Open	
10	29.1	16.1	2.06	21.8	
		11.1	1.21	11.2	
		6.1	1.07	7.0	
		1.1	1.08	7.5	
		-----	1.00	4.2	15.5
10	37.5	24.5	4.20	35.5	
		19.5	1.60	17.0	
		14.5	1.18	10.2	
		9.5	1.18	10.2	
		4.5	1.07	7.0	$\simeq 0$

TABLE 9-b (Continued)

Data on #16 AWG Wire — Vent Tube Open

I (amps)	L (cm)	x (cm)	$\rho x 10^{-8}$ (ohm-cm)	T (°K)	$AdT/dx * x 10^{-3}$
30	29.7	16.7	2.30	47.3	
		11.7	1.29	12.5	
		6.7	1.08	7.5	
		1.7	1.08	7.5	
		----	1.00	4.2	13.1
30	37.3	24.3	3.52	31.8	
		19.3	1.55	16.6	
		14.3	1.17	10.0	
		9.3	1.12	9.0	
		4.3	1.07	7.0	0.1
50	27.4	14.4	1.36	13.8	
		9.4	1.20	10.5	
		4.4	1.09	7.8	
		----	1.09	7.8	
		----	1.00	4.2	21.0
50	37.3	24.3	3.58	32.1	
		19.3	1.56	16.8	
		14.3	1.19	10.2	
		9.3	1.14	9.2	
		4.3	1.09	7.8	$\simeq 0$ +

TABLE 9-b (Continued)

Data on #16 AWG Wire				Vent Tube Open	
I (amps)	L (cm)	x (cm)	$\rho \times 10^{-8}$ (ohm-cm)	T (°K)	$AdT/dx * \times 10^{-3}$
70	27.5	14.5	1.75	18.9	
		9.5	1.25	12.0	
		4.5	1.07	7.0	
		----	1.05	6.0	
		----	1.00	4.2	23.6
70	37.4	24.4	4.08	35.0	
		19.4	1.69	18.0	
		14.4	1.20	11.0	
		9.4	1.12		
		4.4	1.08	7.5	9.2
				Vent Tube Closed	
10	28.8	15.8	2.14	22.5	
		10.8	1.18	10.5	
		5.8	1.08	7.5	
		0.8	1.08	7.5	
		----	1.00	4.2	13.1
10	37.4	24.4	7.51	48.0	
		19.4	2.20	23.0	
		14.4	1.31	13.2	
		9.4	1.22	11.2	
		4.4	1.07	7.0	10.5

TABLE 9-b (Continued)

Data on #16 AWG Wire — Vent Tube Closed

I (amps)	L (cm)	x (cm)	$\rho \times 10^{-8}$ (ohm-cm)	T (°K)	AdT/dx * $\times 10^{-3}$
30	29.2	16.2	2.01	21.3	
		11.2	1.29	11.8	
		6.2	1.08	7.5	
		1.2	1.06	6.5	
		----	1.00	4.2	13.1
30	37.5	24.5	7.26	47.3	
		19.5	2.22	23.1	
		14.5	1.25	12.0	
		9.5	1.14	9.5	
		4.5	1.07	7.0	7.9
50	26.5	13.5	1.96	20.8	
		8.5	1.27	10.0	
		3.5	1.06	6.5	
		----	1.06	6.5	
		----	1.00	4.2	17.0
50	37.5	24.5	7.95	49.5	
		19.5	2.20	23.0	
		14.5	1.30	13.0	
		9.5	1.16	10.0	
		4.5	1.12	9.0	5.9

TABLE 9-b (Continued)

Data on #16 AWG Wire				Vent Tube Closed	
I (amps)	L (cm)	x (cm)	$\rho x10^{-8}$ (ohm-cm)	T (°K)	AdT/dx * x 10^{-3}
70	28.0	15.0	2.03	21.5	
		10.0	1.25	12.0	
		5.0	1.07	7.0	
		0.0	1.07	7.0	
		----	1.00	4.2	17.0
70	37.5	24.5	11.1	57.0	
		19.5	2.66	26.3	
		14.5	1.29	12.9	
		9.5	1.10	13.5	
		4.5	1.07	7.0	15.7

TABLE 9-c

Data on #18 AWG Wire				Vent Tube Open	
10	27.6	14.6	1.59	17.0	
		9.6	1.13	9.5	
		4.6	1.01	5.0	
		----	1.06	6.0	
		----	1.00	4.2	8.7
10	36.9	23.9	4.71	38.0	
		18.9	3.13	29.5	
		13.9	1.40	14.5	
		8.9	1.45	15.5	
		3.9	1.40	14.5	??

TABLE 9-c (Continued)

Data on #18 AWG Wire				Vent Tube Open	
I (amps)	L (cm)	x (cm)	$\rho \times 10^{-8}$ (ohm-cm)	T (°K)	AdT/dx * $\times 10^{-3}$
30	27.5	14.5	6.63	45.0	
		9.5	1.17	10.0	
		4.5	1.03	6.0	
		----	1.04	6.0	
		----	1.00	4.2	10.7
30	36.9	23.9	3.52	32.0	
		18.9	1.43	15.0	
		13.9	1.07	7.0	
		8.9	1.05	6.5	
		3.9	1.04	6.0	12.4
50	27.0	14.0	5.77	42.1	
		9.0	1.66	17.8	
		4.0	1.06	6.5	
		----	1.01	5.0	
		----	1.00	4.2	19.0
50	37.2	24.2	4.52	37.0	
		19.2	1.74	18.8	
		14.2	1.26	13.0	
		9.2	1.19	10.2	
		4.2	1.18	10.0	$\cong 0$

TABLE 9-c (Continued)

Data on #18 AWG Wire				Vent Tube Open	
I (amps)	L (cm)	x (cm)	$\rho \times 10^{-8}$ (ohm-cm)	T (°K)	$A dT/dx$ * $\times 10^{-3}$
30	27.5	14.5	6.63	45.0	
		9.5	1.17	10.0	
		4.5	1.03	6.0	
		----	1.04	6.0	
		----	1.00	4.2	10.7
30	36.9	23.9	3.52	32.0	
		18.9	1.43	15.0	
		13.9	1.07	7.0	
		8.9	1.05	6.5	
		3.9	1.04	6.0	12.4
50	27.0	14.0	5.77	42.1	
		9.0	1.66	17.8	
		4.0	1.06	6.5	
		----	1.01	5.0	
		----	1.00	4.2	19.0
50	37.2	24.2	4.52	37.0	
		19.2	1.74	18.8	
		14.2	1.26	13.0	
		9.2	1.19	10.2	
		4.2	1.18	10.0	$\simeq 0$

TABLE 9-c (Continued)

Data on #18 AWG Wire — Vent Tube Closed

I (amps)	L (cm)	x (cm)	$\rho \times 10^{-8}$ (ohm-cm)	T (°K)	AdT/dx * $\times 10^{-3}$
10	28.3	15.3	6.72	45.5	
		10.3	1.77	19.0	
		5.3	1.43	15.0	
		0.3	1.06	6.5	
		----	1.00	4.2	13.6
10	37.3	24.3	10.8	55.5	
		19.3	3.69	33.8	
		14.3	1.54	16.5	
		9.3	1.47	15.5	
		4.3	1.40	14.5	??
30	28.9	15.9	8.06	50.0	
		10.9	2.02	21.5	
		5.9	1.16	9.8	
		0.9	1.04	5.5	
		----	1.00	4.2	10.7
30	37.2	24.2	8.71	51.6	
		19.2	2.28	23.5	
		14.2	1.22	11.5	
		9.2	1.17	10.0	
		4.2	1.13	9.0	2.1

TABLE 9-c (Continued)

Data on #18 AWG Wire				Vent Tube Closed	
I (amps)	L (cm)	x (cm)	$\rho \times 10^{-8}$ (ohm-cm)	T (°K)	AdT/dx * $\times 10^{-3}$
50	29.1	VERY RAPID BOILING OF THE HELIUM			
50	37.4	24.4	10.4	55.5	
		19.4	3.12	28.8	
		14.4	1.43	15.0	
		9.4	1.26	13.0	
		4.4	1.17	9.7	4.5

TABLE 9-d

Data on #20 AWG Wire				Vent Tube Open	
10	28.0	15.0	4.10	35.0	
		10.0	1.45	15.1	
		5.0	1.05	6.5	
		0.0	1.02	5.5	
		----	1.00	4.2	9.3
10	37.7	24.7	3.41	31.0	
		19.7	1.45	15.0	
		14.7	1.07	7.0	
		9.7	1.07	7.0	
		4.7	1.05	6.5	7.6

TABLE 9-d (Continued)

Data on #20 AWG Wire				Vent Tube Open	
I (amps)	L (cm)	x (cm)	$\rho \times 10^{-8}$ (ohm-cm)	T (°K)	AdT/dx * $\times 10^{-3}$
20	27.5	14.5	3.86	33.8	
		9.5	1.45	15.6	
		4.5	1.05	6.0	
		----	1.02	5.0	
		0000	1.00	4.2	10.0
20	38.0	25.0	3.13	29.5	
		20.0	1.37	14.0	
		15.0	1.12	9.0	
		10.0	1.10	8.4	
		5.0	1.09	7.7	3.6
30	27.5	14.5	3.76	33.0	
		9.5	1.35	13.6	
		4.5	1.06	6.5	
		----	1.03	5.5	
		----	1.00	4.2	8.8
30	38.0	25.0	2.79	27.0	
		20.0	1.33	13.5	
		15.0	1.10	8.5	
		10.0	1.09	7.9	
		5.0	1.09	7.9	5.3

TABLE 9-d (Continued)

Data on #20 AWG Wire				Vent Tube Open	
I (amps)	L (cm)	x (cm)	$\rho \times 10^{-8}$ (ohm-cm)	T (°K)	AdT/dx * $\times 10^{-3}$
40	38.0	25.0	2.40	24.5	
		20.0	1.28	12.5	
		15.0	1.11	8.5	
		10.0	1.10	8.2	
		5.0	1.09	7.8	4.2
				Vent Tube Closed	
10	29.0	16.0	2.45	25.0	
		11.0	1.27	12.5	
		6.0	1.05	6.5	
		1.0	1.03	6.0	
		----	1.00	4.2	6.7
10	38.2	25.2	3.73	33.0	
		20.2	1.48	15.5	
		15.2	1.11	8.8	
		10.2	1.03	6.0	
		5.2	1.05	6.5	5.7
20	28.8	15.8	2.93	28.0	
		10.8	1.29	12.8	
		5.8	1.05	6.5	
		0.8	1.02	5.0	
		----	1.00	4.2	6.7

TABLE 9-d (Continued)

Data on #20 AWG Wire — Vent Tube Closed

I (amps)	L (cm)	x (cm)	$\rho \times 10^{-8}$ (ohm-cm)	T (°K)	AdT/dx * $\times 10^{-3}$
20	38.5	25.5	4.66	38.0	
		20.5	1.58	17.0	
		15.5	1.14	9.5	
		10.5	1.07	7.0	
		5.5	1.05	6.5	5.7
30	28.5	15.5	3.51	32.0	
		10.5	1.34	13.7	
		5.5	1.02	5.2	
		0.5	1.04	6.0	
		----	1.00	4.2	8.8
30	39.5	26.5	1.84	19.8	
		21.5	1.14	9.3	
		16.5	1.05	6.0	
		11.5	1.05	6.0	
		6.5	1.03	5.0	7.3
40	39.8	VERY RAPID BOILING OF LIQUID HELIUM			

TABLE 9-e

Data on #22 AWG Wire — Vent Tube Open

I (amps)	L (cm)	x (cm)	$\rho \times 10^{-8}$ (ohm-cm)	T (°K)	AdT/dx * $\times 10^{-3}$
5	27.7	14.7	4.81	38.6	
		9.7	1.37	14.0	
		4.7	1.05	6.0	
		----	1.02	5.0	
		----	1.00	4.2	5.9
10	29.1	16.1	4.96	39.0	
		11.1	1.57	16.5	
		6.1	1.05	6.6	
		1.1	1.04	6.5	
		----	1.00	4.2	5.5
20	29.2	16.2	5.16	40.0	
		11.2	1.54	16.5	
		6.2	1.03	5.5	
		1.2	1.04	6.0	
		----	1.00	4.2	9.1

TABLE 9-e (Continued)

Data on #22 AWG Wire — Vent Tube Closed

I (amps)	L (cm)	x (cm)	$\rho \times 10^{-8}$ (ohm-cm)	T (°K)	AdT/dx * $\times 10^{-3}$
5	27.8	14.8	5.15	40.0	
		9.8	1.53	16.5	
		4.8	1.06	6.5	
		----	1.00	4.2	
		----	1.00	4.2	5.9
10	28.5	15.5	4.85	39.0	
		10.5	1.56	16.0	
		5.5	1.07	7.0	
		0.5	1.05	6.5	
		----	1.00	4.2	5.9
20	28.8	15.8	.534	40.8	
		10.8	1.60	17.0	
		5.8	1.07	7.0	
		0.8	1.08	7.5	
		----	1.00	4.2	5.9
30	28.9	15.9	5.79	42.5	
		10.9	1.58	17.0	
		5.9	1.04	6.0	
		0.9	1.03	5.5	
		----	1.00	4.2	5.9

TABLE 9-f

Data on #24 AWG Wire — Vent Tube Open

I (amps)	L (cm)	x (cm)	$\rho \times 10^{-8}$ (ohm-cm)	T (°K)	AdT/dx * $\times 10^{-3}$
5	28.2	15.2	2.03	21.2	
		10.2	1.10	8.3	
		5.2	1.04	5.5	
		0.2	1.00	4.2	
		----	1.00	4.2	4.0
10	28.3	15.3	2.22	23.0	
		10.3	1.13	9.0	
		5.3	1.04	6.5	
		0.3	1.03	6.0	
		----	1.00	4.2	2.7
15	27.9	14.9	1.77	19.0	
		9.9	1.09	7.8	
		4.9	1.04	5.5	
		----	1.00	4.2	4.0
20	28.0	15.0	2.02	21.5	
		10.0	1.09	7.8	
		5.0	1.03	5.5	
		0.0	1.03	5.0	
		----	1.00	4.2	3.5

TABLE 9-f (Continued)

Data on #24 AWG Wire — Vent Tube Closed

I (amps)	L (cm)	x (cm)	$\rho \times 10^{-8}$ (ohm-cm)	T (°K)	AdT/dx * $\times 10^{-3}$
5	28.5	15.5	3.29	30.2	
		10.5	1.32	13.2	
		5.5	1.04	5.5	
		0.5	1.00	4.2	
		----	1.00	4.3	3.9
10	28.8	15.8	4.34	36.0	
		10.8	1.47	15.5	
		5.8	1.06	7.0	
		0.8	1.03	6.0	
		----	1.00	4.2	3.1
15	29.0	16.0	5.95	43.0	
		11.0	1.65	17.8	
		6.0	1.08	7.5	
		1.0	1.04	5.5	
		----	1.00	4.2	3.9

*The value of dT/dx was determined at the point

where T = 10°K

?? = unable to determine AdT/dx from the Tvs. x plot

TABLE 10

Observations from Figure 17

Current (amps	Optimum wire size
5	smaller than #24 AWG
10	#24 or smaller
15	insufficient data
20	probably #24
30	probably #22
40	#20 or larger
50	#16 or #18
70	possibly #14
From Sobel and McNichol /3/:	
0.5	#38
1.0	#34

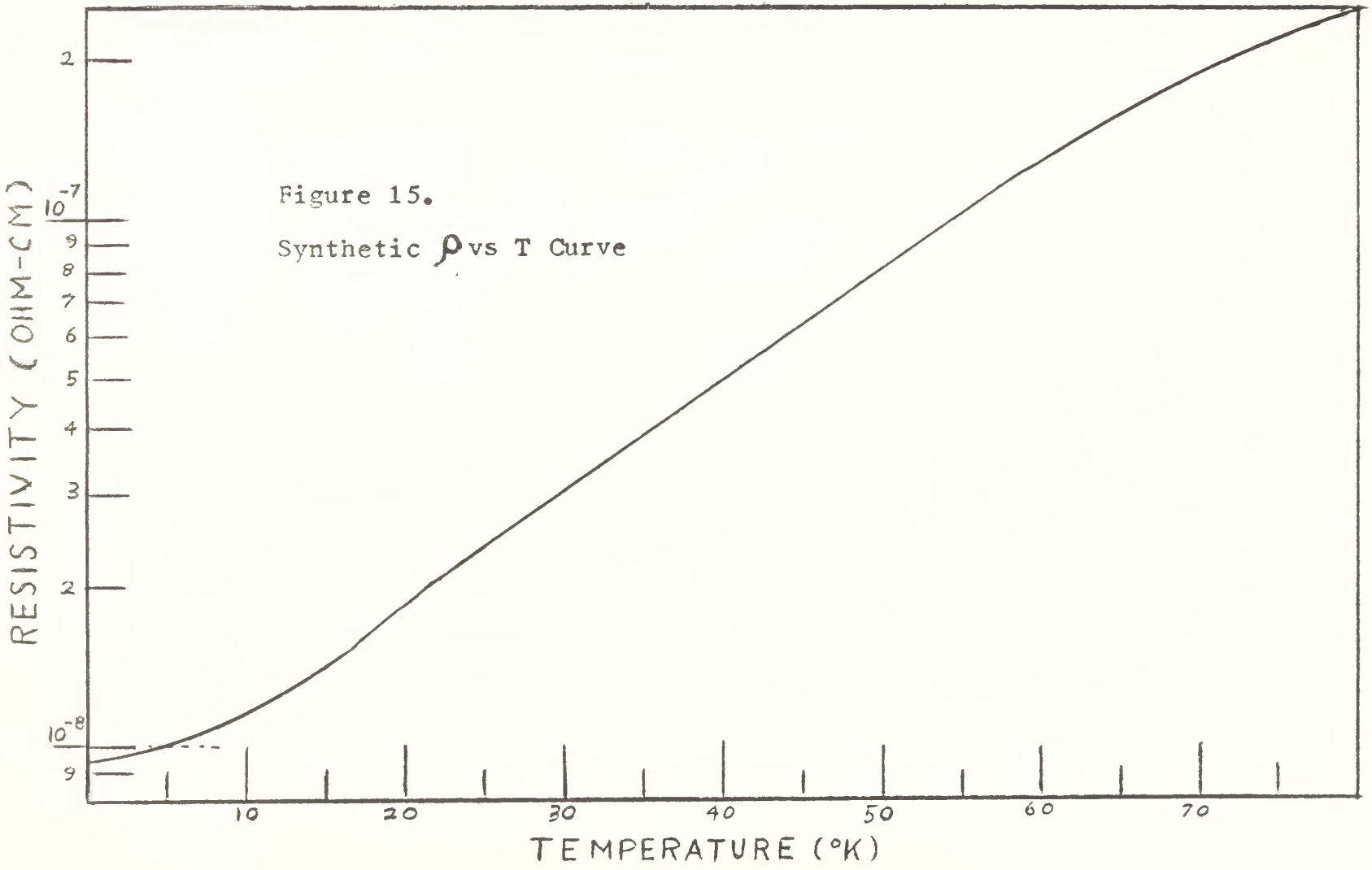

Figure 15.

Synthetic ρ vs T Curve

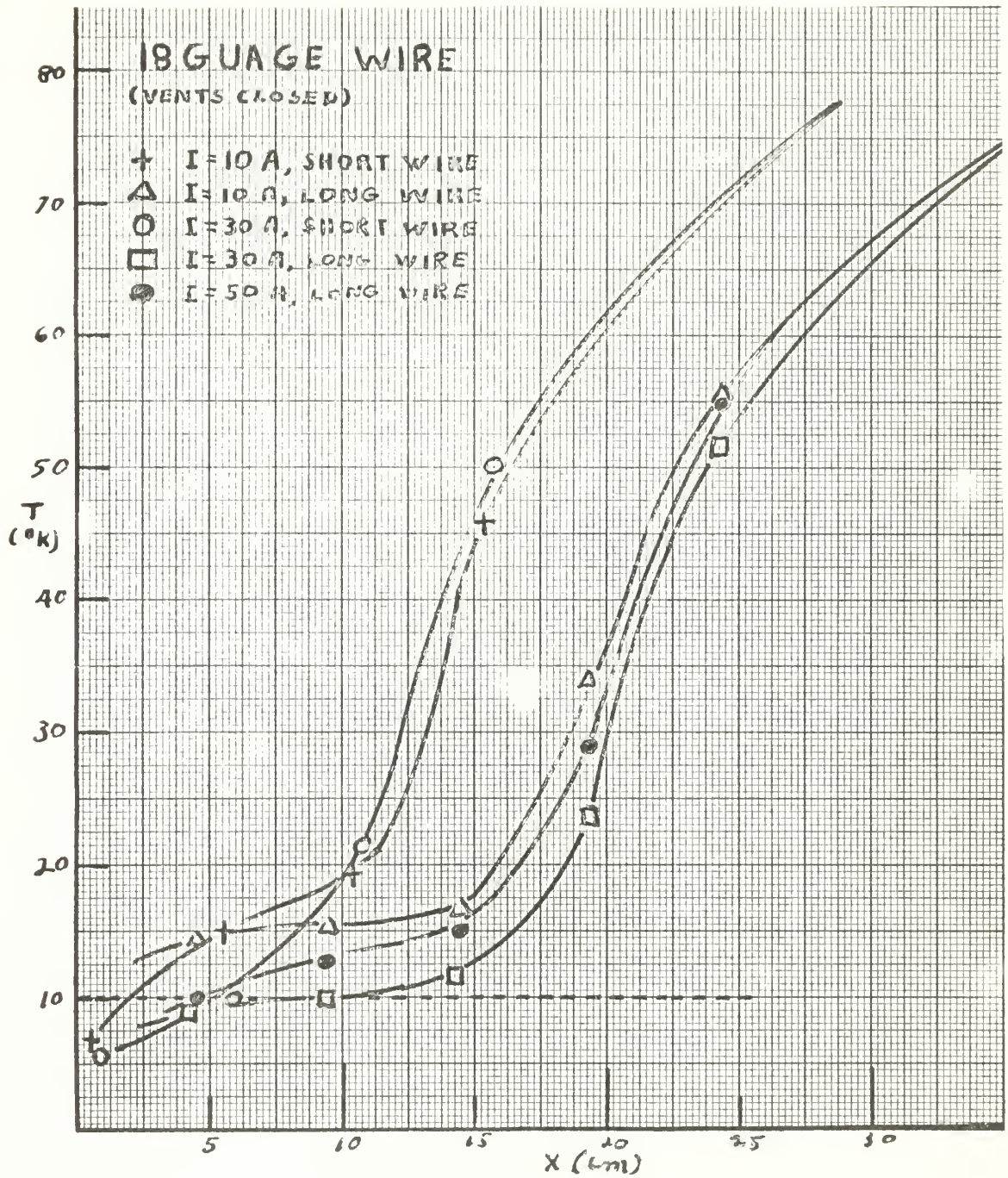

Figure 16.

Example T vs x Curves

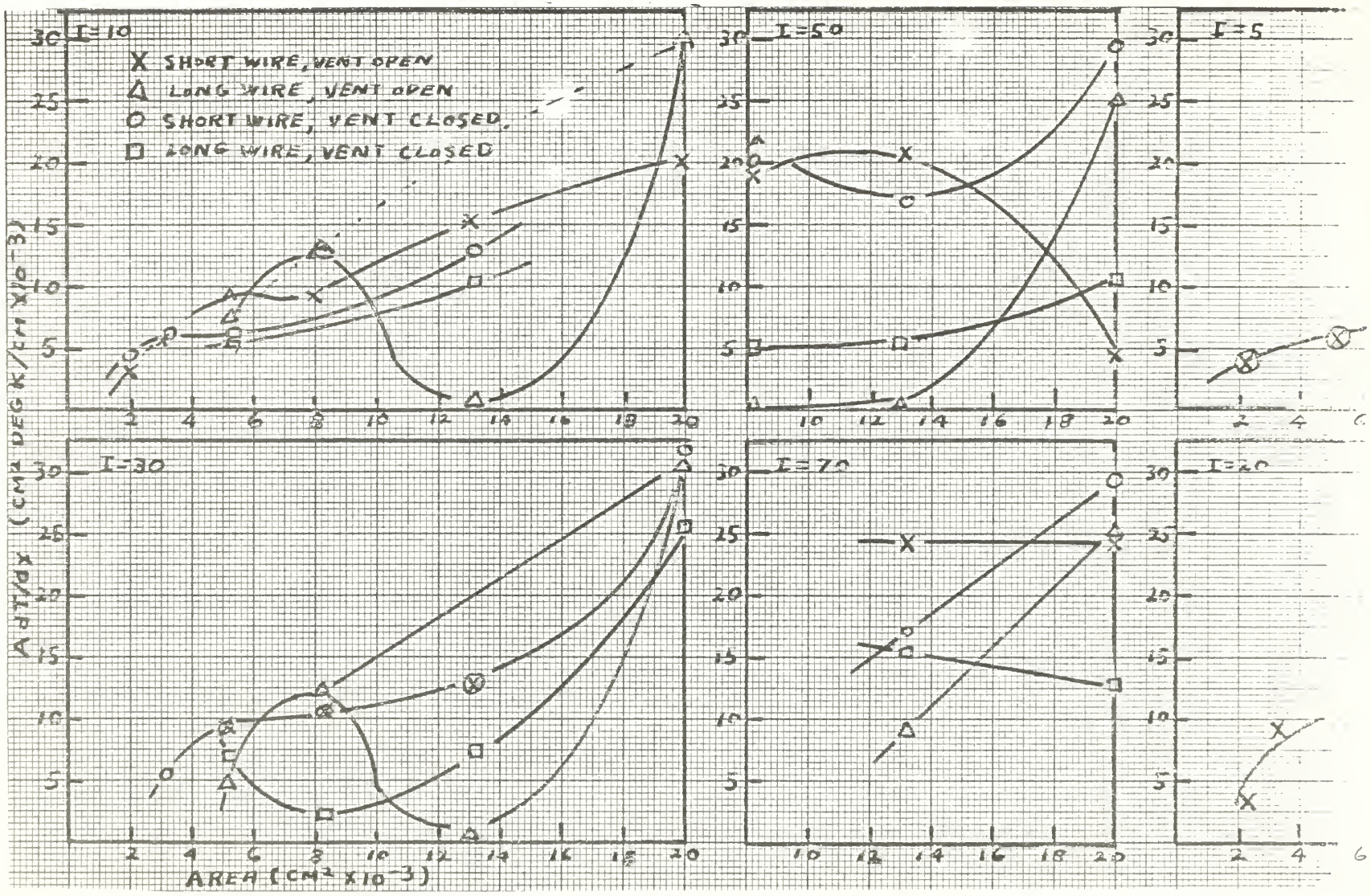

Figure 17. AdT/dx Curves at T = 10°K

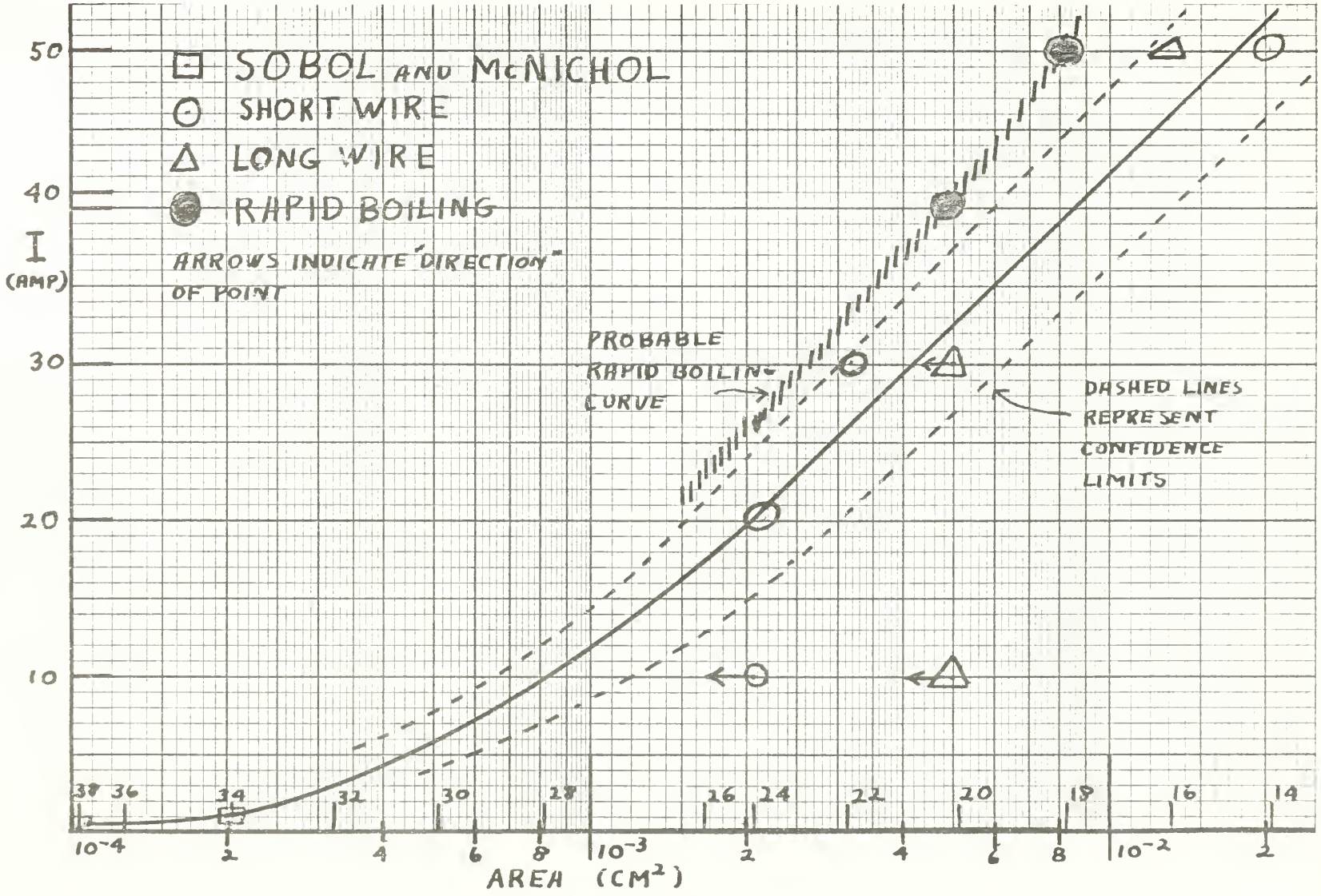

Figure 18. Current vs Optimum Lead Size

APPENDIX II

CONNECTORS TO SUPERCONDUCTING WIRE

The first attempt at making high current connection between copper conductor and superconducting wire consisted of mechanically squeezing the Nb_3Zr wire between strips of copper.

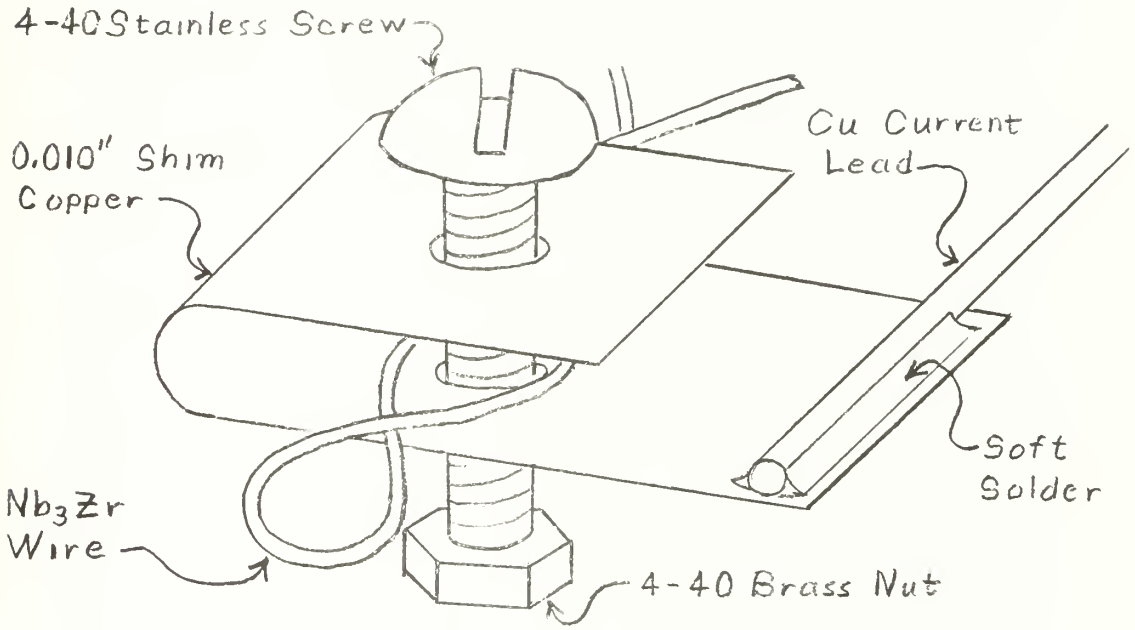

Fig. 29

The Nb_3Zr wire was first cleaned of all the enamel and then etched for about one minute in a HF - HNO_3, acid solution consisting of:

5% Hydrofloric Acid (HF)

45% Nitric Acid (HNO_3)

50% Distilled Water

As soon as the wire was removed from the acid it was rapidly rinsed with distilled water and then tightly clamped in the copper "sandwich". The copper was cleaned in Nitric Acid just prior to making the connection.

Care was taken to be sure that the Nb_3Zr wire was laid close to the body of the screw so that the head of the screw would squeeze as much of the wire as possible. The screws were tightened to the point just short of

stripping the threads of the nuts to insure that the superconducting wire was deeply impressed into the copper.

This type of connector, when tested with a hair pin of Nb_3Zr wire, passed a current of about 34 amps before going normal. When two of these connectors were used in parallel for the same connection, 64 amperes was carried without going normal. (This was all the current our power supply would produce at the time.)

These connectors were used in the first data run with the first coil. We believe that many of the limitations of the first coil were possibly due to these connectors.

For the remainder of the project an improved connector was developed which consisted of electro-plating the Nb_3Zr wire with copper so that ordinary solder joints could be made to it.

We feel that plating the superconducting wire makes a better joint since it helps prevent possible contamination of the copper-superconducting interface. It also provides a more intimate contact between the superconducting and the copper conductor, and permits this contact to be made over a larger surface area.

Originally, copper was plated directly onto the Nb_3Zr wire. The wire was first etched for about 1.5 minutes in the previously described acid solution and then immediately placed in an acid copper plating bath. (Note: All electro-plating was done at the rate of 0.03 amp/cm^2 over a length of about one to 1-1/2" of wire.)

A handbook method /10/ for nickel plating of niobium was tried without success. It involved anodic etching the wire in a NaOH solution and then plating it in a Woods nickel strike bath.

A reasonably successful method of nickel plating was developed by

modifying a method published /10/ for zirconium. This modified technique was:

1. Clean all enamel and tarnish off of wire by light sanding.
2. Clean by soaking in clean acetone. From this point on, do not touch the clean wire.
3. Rinse in distilled water.
4. Etch in the wire $HF-HNO_3$ acid solution for about one minute.
5. Place immediately in Watts Nickel Plating bath at PH 2.5, 60 degrees C., with a current of approximately 0.03 to 0.04 amp/cm(1). Plate for about 1-1/2 minutes.
6. Remove the wire from the Ni bath and place it in a copper acid bath at 40 degrees C. and current of 0.03 amp/cm(1). After about 15-20 seconds remove the wire and inspect the copper plating. If it is splotchy or not uniform clean the wire down to bare Nb_3Zr and start over. If the plating seems satisfactory, continue plating for approximately 30 minutes, (more time will not hurt.)

Soldered connectors were made up using this type of plating and 3/8" wide copper strips (the same method as for the copper only plating.) Care was taken to insure good tinning of the wire, and to insure that the solder uniformly flowed around the Nb_3Zr wire while still keeping as close contact between the wire and copper strip as possible.

(1) The plating voltage should be connected to the wire before it is is placed in the plating solution. It is best to connect it before etching so that no time is wasted in getting the wire from the acid to the N_i bath.

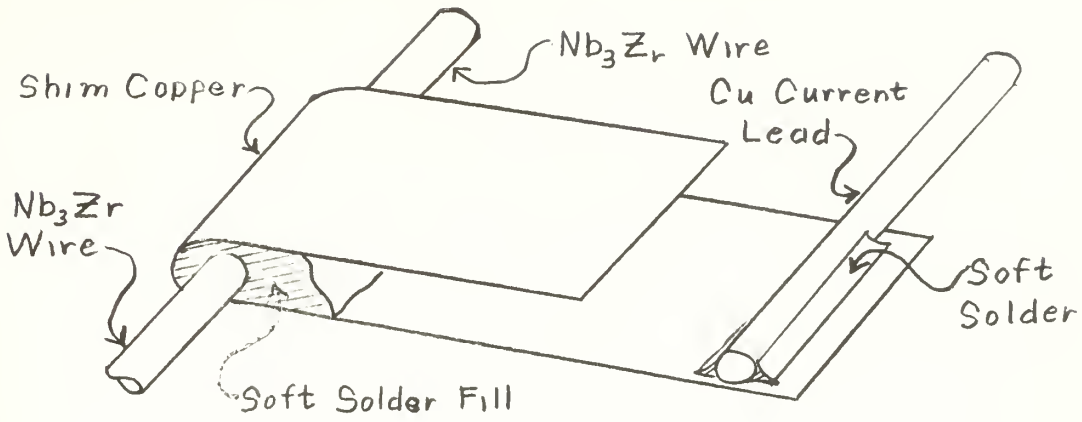

Fig. 20

A connector of this type, using three minutes of Cu plating, passed 50 amperes before going normal. (This may have been a lower current than the connector was actually capable of handling since the liquid Helium level was quite low at the time of the test and the wire may have been above the Helium level.) A similar connector with 30 minuteCu plating carried 100 amperes (the limit of our power supply) without going normal. The nickel - copper connectors (with 30 minute copper plating) were used for all of the rest of our test runs of the magnet. On the second magnet, tubular crimp-on spade lug connectors were used instead of a folded copper strip for connecting to the plated wire.

Three spade lugs were slipped, in series, over the tinned and plated Nb_3Zr wire. The lugs were then filled with soft solder and crimped while the solder was still molten. The individual spade lugs were then soldered together to provide continuity of the conventional conductor. This method provided approximately an inch of intimate superconductor-copper connection in addition to providing a convenient means of connecting to the current leads via the spade lugs.

WATTS TYPE NICKEL BATH:

	gm/liter
Nickel sulfate $NiSO_4 . 6H_2O$	310
Nickel Chloride $NiCl_2 . 6H_2O$	45
Boric Acid	30 to 40

ACID COPPER BATH:

	gm/liter	cc/liter
Copper Sulfate $CuSO_4 . 5H_2O$	208	
Sulfuric Acid (Sp. Gr. I. 84)H_2SO_4		33

Orthophenosulfonic Acid (Igm/liter) may be added to toughen the deposit. This bath produces a hard deposit. It may be made softer by raising the temperature.

No attempt was made to plate copper directly onto Nb_3Zr using an alkaline solution (copper cyanide) since the materials were not readily available. This method might be worthy of further investigation.

APPENDIX III

THE THERMAL EXPANSION COEFFICIENT OF Nb_3Zr

A simple experiment was conducted to determine the thermal expansion coefficient of the Nb_3Zr wire. The apparatus consisted of a block of STYROFOAM in which a rectangular bowl was cut. The Nb_3Zr wire was punched through the STYROFOAM at one end. The STYROFOAM block was attached to a wooden 1" x 6" board. The Nb_3Zr was attached to a nail that penetrated the STYROFOAM into the wood at one end of the bowl. Constant tension was maintained on the other end of the Nb_3Zr wire by a pully and a 500 gram weight. Figure 21 shows this apparatus. Liquid nitrogen was put into the bowl. The length of contraction of the wire was determined by measuring the movement of a reference mark on the wire just outside the STYROFOAM. These measurements were made with a horizontal traveling vernier microscope. Table 11 lists the data taken. The length of wire cooled by the liquid nitrogen was estimated to be 36.6 cm.

Runs were made on copper wire and soft steel wire to check the accuracy of the apparatus. The data was read as quickly as possible after cooling. It was found that the reading would change abruptly after about a second after initial contraction. This was attributed to contractions within the apparatus itself.

From Scott /12/, the value of $\Delta L/L$ for copper between the temperatures of 294°K and 77°K is 305×10^{-5} and for 1020 steel between the same temperatures is 192×10^{-5}. We made no attempt to check the results further. The experiment yielded the information that Nb_3Zr in cooling from room temperature to liquid nitrogen temperature will have a contraction ratio of $\Delta L/L = 160 \times 10^{-5}$. Since most materials undergo approximately 90% of their

contraction in these temperature ranges, we conclude that upon cooling to liquid helium temperatures from room temperature the contraction ratio for Nb_3Zr is approximately $186 \pm 10 \times 10^{-5}$.

This part of the thesis has not been an attempt to determine the thermal expansion coefficient accurately, but rather to get a working number to be applied to the design of magnets employing the wire. Such was accomplished.

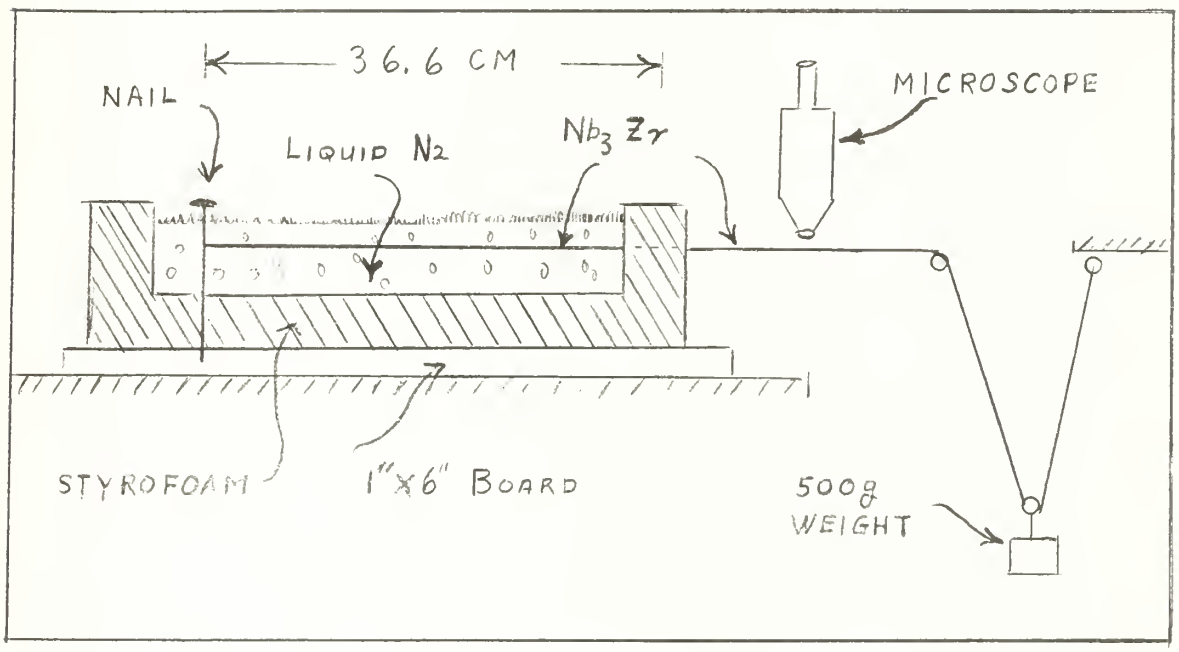

Fig. 21

TABLE 11

Data Taken on Thermal Contraction from 294°K to 77°K

Material	$\Delta L_{(cm)}$	$\Delta L/L \times 10^{-5}$	Mean for the material
copper	0.1195	336	
	0.1271	357	
	0.1179	331	
	0.1129	317	335 ± 21
soft steel	0.0820	224	
	0.0620	170	197 ± 38
Nb_3Zr	0.0615	168	
	0.0545	419	
	0.0578	158	
	0.0595	162	
	0.0600	164	160 ± 10

APPENDIX IV

CALCULATIONS OF FIELDS IN THE SOLENOIDS

Two methods were used to calculate the field in the solenoid.

For relatively thin layers of windings, the infinitely thin current sheet approximation was used.

$$H_{o_2} = \frac{2\pi}{10} \frac{N}{2b} I \, (\sin\alpha + \sin\beta) \quad \text{gauss}$$

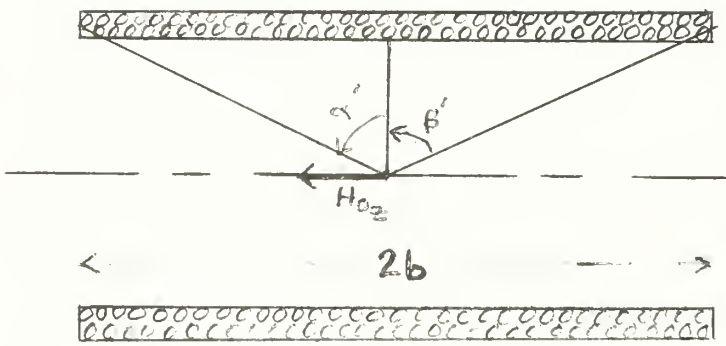

N = total number of turns.
2b = length of Solenoid in cm.
I = Current in wire in amperes.

Fig. 22

In this case, all the turns were assumed to lie in a layer at the mean radius of the actual winding.

Sample calculation:

Layers A_1 through A_4 of the first coil.

length = 3.475" = 8.826 cm.

inside diameter = 3.070"
outside diameter = 3.184"
} mean diameter = 3.127"

N = 614 turns

$\alpha' = \beta' =$ [illegible] $= 48.1°$ $\therefore \sin\alpha' = 0.742$

$H_{oz} = (2\pi/10)(N/4b)\, I\, 2\sin\alpha' = (2\pi/10)(614/3.924)\, I\,(0.742)$

$\therefore H_{oz} = 6.531\ I$ gauss $= 0.00653\ I$ K-gauss

For the thicker sets of windings, the formula [1]

$$H_{oz} = (4\pi/10)\, b\, i\lambda \ln\left(\frac{\alpha + \sqrt{\alpha^2+\beta^2}}{1+\sqrt{1+\beta^2}}\right) \text{ gauss}$$

was used. This formula is the field at the center of a square ended solenoid that is obtained by integrating:

$$dH_o = (2\pi/10)\, i\lambda\,(r^2/(r^2+z^2)^{3/2})\, dr\, dz$$

which is the field generated by an infinitesimal loop at (r,Z).

Here b = 1/2 length of solenoid in cm.

$i\lambda = I\,[illegible]$

I = current in wire (amperes)

A = cross sectional area allowed per conductor

$= (a_2 - a_1)\, 2b/N$ cm^2/turn

$\alpha = \frac{a_2}{a_1} = \frac{\text{outer radius}}{\text{inner radius}}$

$\beta = [illegible] = \frac{\text{half length}}{\text{inner radius}}$

By substitution:

$$H_{oz} = (4\pi/10)(I\, b/A) \ln\left(\frac{\alpha + \sqrt{\alpha^2+\beta^2}}{1+\sqrt{1+\beta^2}}\right) \text{ gauss, cm, amperes.}$$

This relationship is to be favored over the single - layer approximation only for thick coils because a slight variation in α at small values can cause greatly varying results.

Example:

Field for entire second coil.

$2b = 8.826$ cm, $b = 4.413$

$a_1 = 3.899$ cm

$a_2 = 4.775$ cm

$N = 3957$ turns

$\alpha = 4.775/3.899 = 1.225$, $\alpha^2 = 1.5006$

$\beta = 4.413/3.899 = 1.132$, $\beta^2 = 1.2814$

$$A = \frac{(a_1 - a_2)2b}{N} = 1.95 \times 10^{-3} \text{ cm}^2/\text{turn}$$

$$H_{oz} = (4\pi/10)(4.413 \text{ cm})(1.95 \times 10^{-3} \text{ cm}^2/\text{turn})\, I \ln\left(\frac{1.225 + \sqrt{1.5006 + 1.2814}}{1 + \sqrt{1 + 1.2814}}\right)$$

$= 403I$ gauss

The ratio of $\frac{H_{max}}{H_{oz}} = K$ was found from a plot of constant values of K vs. α & β . /1/

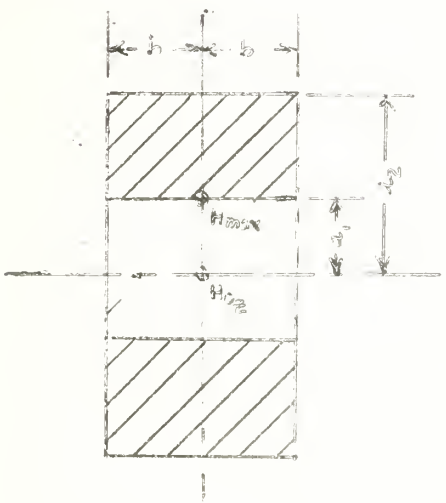

Example ; Entire 2nd Coil

$K = 1.13$

$H_{oz} = 403\,I$

$H_{max} = 1.13 \times 403I = 455\,I$ gauss

Fig. 23

Approximate field contours were found by extrapolation of field contours presented by Boom & Livingston /1/ for coils with various values of α & β . The estimated field contours for the second solenoid are shown in Fig. 24.

The mean field intensity within the solenoid was estimated by dividing the volume within the solenoid into rings with a 1 cm square cross section. The average field intensity for each ring, as estimated from the field contour plot, was multiplied by the volume of that ring. All of the (field intensity) X(volume) products were summed and then divided by the total volume within the solenoid.

This calculation of the mean magnetic field intensity resulted in a value of $\overline{H} = 0.95\ (H_{center})$.

The inductance of the second coil was calculated using two empirical formulas. (See just below Fig. 24 for these calculations). The two values of inductance so calculated were $L = 0.778$ henry and $L = 0.82$ henry.

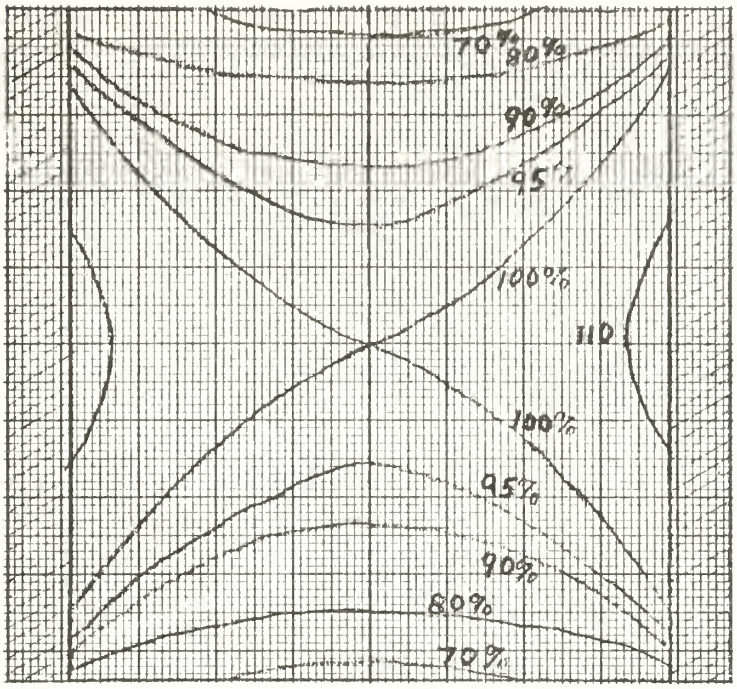

Figure 24
Plot of Equal Field Intensity Contours of 2nd Magnet in Terms of Percent of Field Strength at Center of Coil

CALCULATION OF INDUCTANCE OF 2nd SOLENOID

$$L = \frac{0.2a^2n^2}{3a+9b+10c} = 820{,}000\ \mu h$$

Where: a=Average diameter in inches, b=Length in inches,
c=Radial depth of windings in inches,
n= Total number of turns. /13/

OR

$$L = L_s - \frac{0.0216\ n^2 ac}{b}\ (\ 0.693 + B_s) = 0.778 \times 10^6\ \mu h.$$

Where: $L_s = \frac{0.0395\ a^2 n^2}{b} K$

$K = 0.6922, \quad B_s = 0.2797$

a=Average radius in cm., b=Length in cm.
c=Radial depth of windings in cm.
n=Total number of turns. /14/

TABLE 12

Calculated H/I used in finding H for both coils

		Coil Number One
Loops (A or B)	H/I* (at center)	H/I* (Max. in windings)
1	0.0155	0.0174
2	0.0162	0.0182
3	0.0160	0.0181
4	0.0176	0.0199
1-2	0.0318	0.0356
1-3	0.0478	0.0536
1-4	0.0653	0.0733
1-12 (B only)	0.1971	0.1989
1-13 (A only)	0.2307	0.2607
2-7	0.0999	0.1124
3-4	0.0336	0.0389
		Coil Number Two
A	0.216	0.243
B	0.185	0.208
A&B	0.401	0.451

* H is in units of K-gauss

I is in units of Amperes

APPENDIX V

GAUSS METER

For the purpose of getting a quick estimate of the magnetic field intensity, while testing the superconducting solenoid, a simple gauss meter was devised.

Basically the device consisted of a small coil which was quickly rotated 180° in the magnetic field, the resulting charge that was induced to flow was measured by a ballistic galvanometer thereby giving a measure of the field intensity.

The coil was a 0.8cm. by 1 cm. rectangular loop of about 40 turns taken from an old R.F. ammeter (thermocouple type). The coil, its springs and its bearings were all carefully removed from the meter. The two jeweled bearing mounts were then mounted in two pieces of LUCITE which were in turn mounted on a fiber tube. A one inch long hard brass wire was then cemented to the coil perpendicular to the coil's axis of rotation so that the wire protruded equally from each side of the coil. The coil was then mounted in its newly mounted bearings and the original springs were re-connected to provide electrical connections to the coil and to provide a "re-centering" torque for the coil.

A thin rod was ther mounted through the LUCITE so that it, in combination with the previously mentioned brass wire, would provide a stop which would limit the coil's rotations to 180°.

When arranged for operation, the plane of the coil would be oriented perpendicular to the field to be measured. The coil would thereby be subjected to a torque and would rotate 180° against its springs. The current

and springs should be adjusted to provide essentially 180° of rotation. (70 ma current was found to be sufficient in fields of 1 K-gauss or more.) To measure the field, the current passing through the coil would be shut off and the coil would be immediately placed across a ballistic galvonometer. The coil would then rotate 180° back to rest due to the torque from its springs, a charge would be induced to flow and the galvanometer would deflect. (See Fig. 26 for a schematic diagram of the circuit). A resistance, R, could be placed in series with the galvanometer to permit the range of the device to be extended.

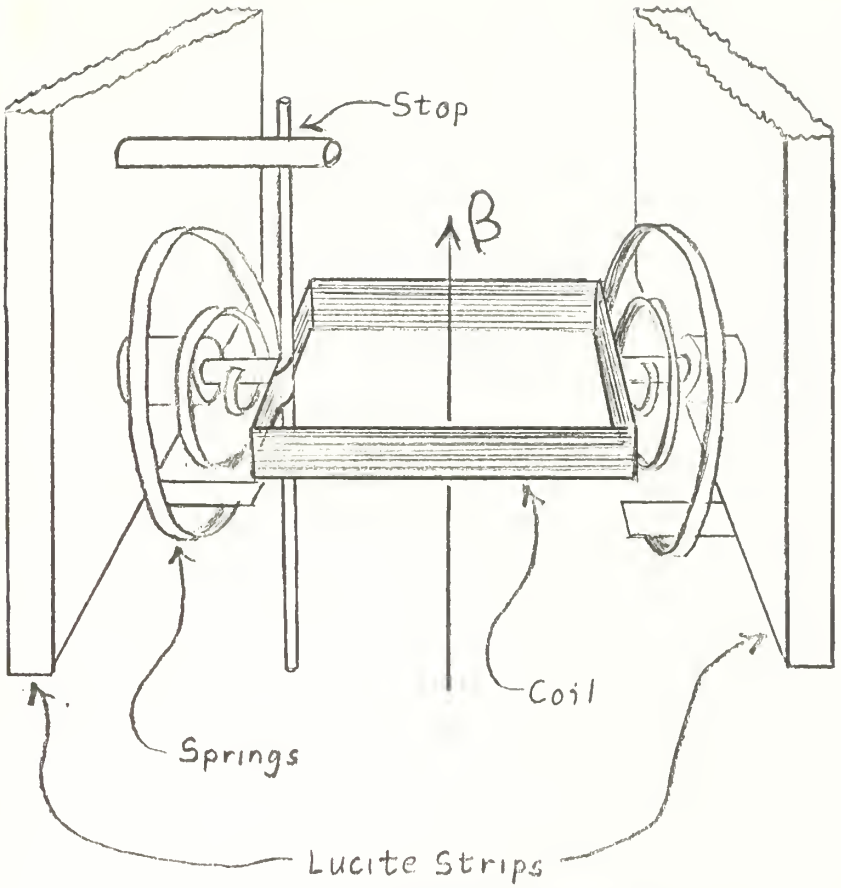

Figure 25
Flip Coil
Gauss Meter

Schematic of Gauss Meter
Figure 26

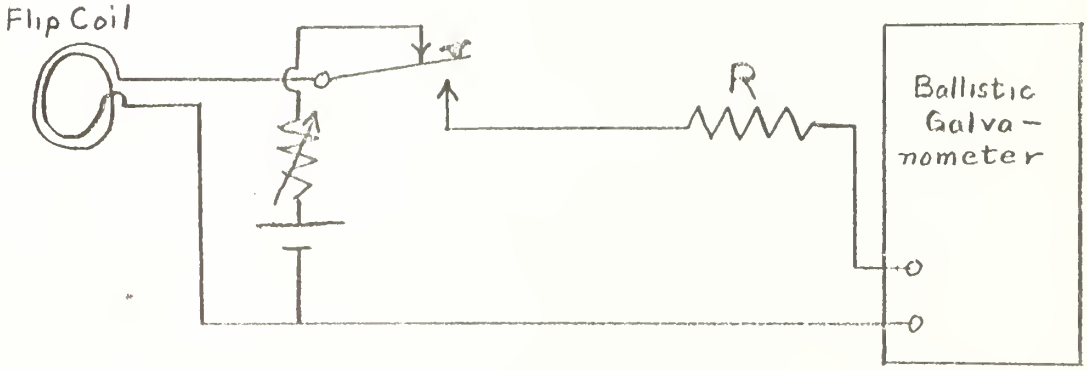

APPENDIX VI

THE MAGNETIC COOLING DEVICE

In another project at the United States Naval Postgraduate School, preparations were being made for the study of phonon excitation of a Ruby maser. It was estimated that a population density difference of only 2 or 3% was possible with the temperatures obtainable from helium pumping; therefore, further cooling of the maser was desirable. This naturally led to the consideration of an adiabatic demagnetization cooling device. The primary requirements on this device were that it had to be able to fit within the limited cryostat space available for the maser experiment. The size of the magnet for the cooling device had to be of the same order of magnitude as the cryostat since most of the space external to the cryostat was taken up by a large electromagnet used to apply fields to the maser. And the device had to be able to provide a reasonable improvement in cooling over what was possible with helium pumping.

The recent development of superconducting alloys capable of carrying high currents in high magnetic fields seemed to provide a solution to our requirements for a magnet for the cooling device. On the basis of information published by Boom & Livingston /1/, it was considered feasible to construct a superconducting solenoid which could be placed inside of the master's cryostat, and could provide sufficient field to satisfactorily operate the cooling device.

The proposed cooling device will consist of the superconducting solenoid as described in this thesis with a single crystal of ferric ammonium alum situated inside the solenoid to provide the working medium. (See Fig. 27) The crystal is to be cut in the shape of a cylinder so that it fills

the volume inside of the solenoid. A hole is cut through the center of the salt crystal (See Fig. 28) to provide for the passage of waveguides, etc., from the maser, which is about 15" below the salt.

Thermal contact between the salt and the maser is provided by 39 ultra pure silver wires, 0.02 inches in diameter, which are to be soldered to the ruby at one end and are grown into the salt crystal at the other end. Additional thermal contact between the salt and the wire is provided by a mesh of fine silver ribbons inside the crystal, which are spot welded to the silver wires. There will be a stainless steel "can" which will separate the solenoid and its helium bath from the salt, waveguides, and maser-all of which will be in a vacuum.

Ferric ammonium alum was selected for the working medium in the device primarily because it is the most commonly used material for this purpose, information about it was readily available, and it was commercially available at moderate cost.

The Iron Alum entropy temperature diagram for constant magnetic field was taken from Heer, Barnes and Daunt /5/. Daunt's data only goes up to 1.2°K, the curves at temperatures above this represent an extrapolation we made of this data.

Although Daunt's curve only goes up to 1.2°K we feel safe in extrapolating it to slightly above 2°K since the entropy due to the lattice is still quite small and would introduce negligible error. Garrett /6/ claims that the lattice entropy is usually of the order of $100T^3$ erg/gm°K. For ferric ammonium alumn, this makes

$$\left(\frac{S}{R}\right)_{LATTICE} = \frac{100\,T^3 \times 482\ gm/mole}{8.314 \times 10^7\ erg/mole°K} = 1.8 \times 10^{-4}\,T^3$$

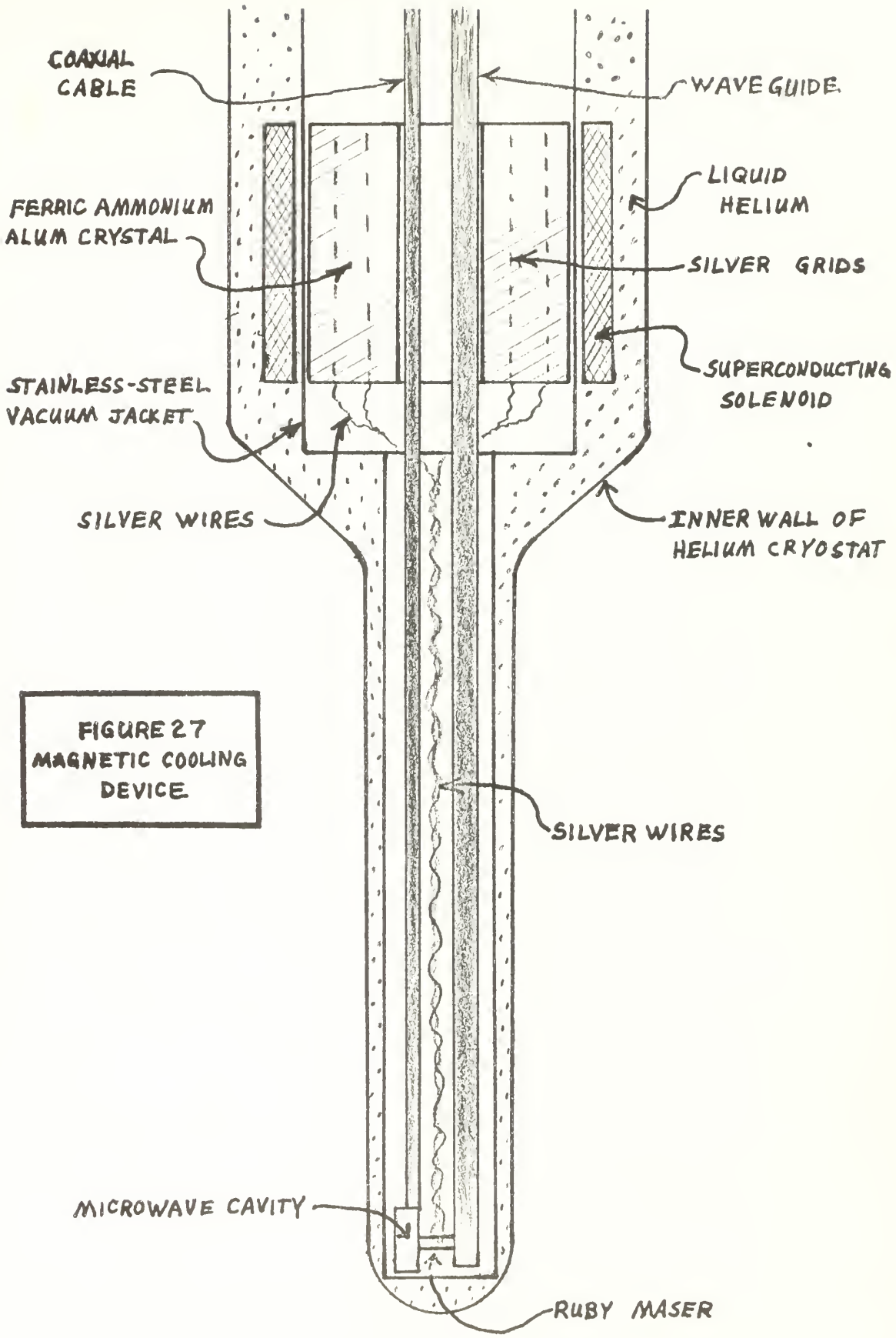

FIGURE 27
MAGNETIC COOLING DEVICE

FIGURE 28

CROSS SECTION OF SALT CRYSTAL

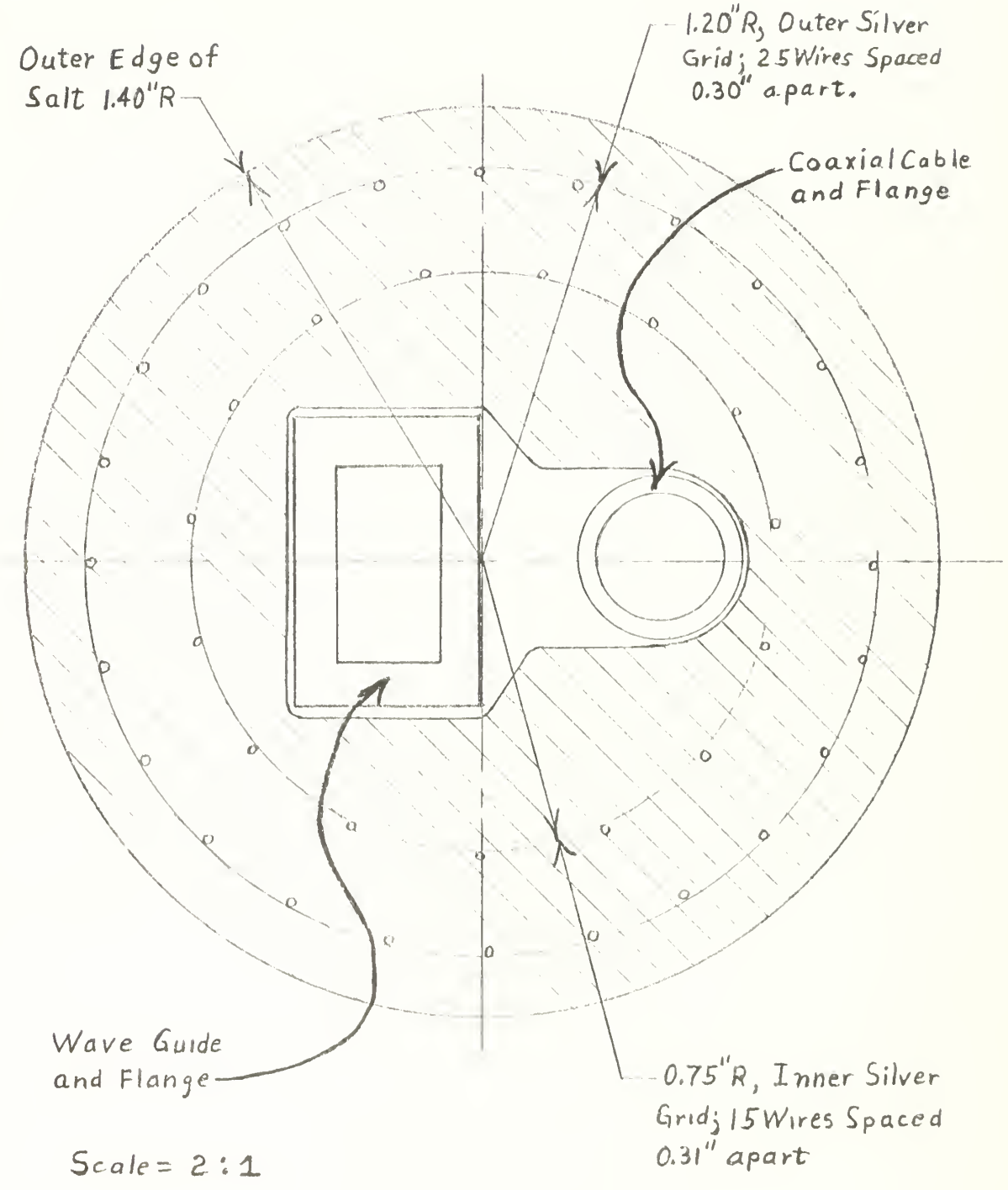

FIGURE 29
ENTROPY vs TEMPERATURE
FOR FERRIC AMMONIUM ALUM

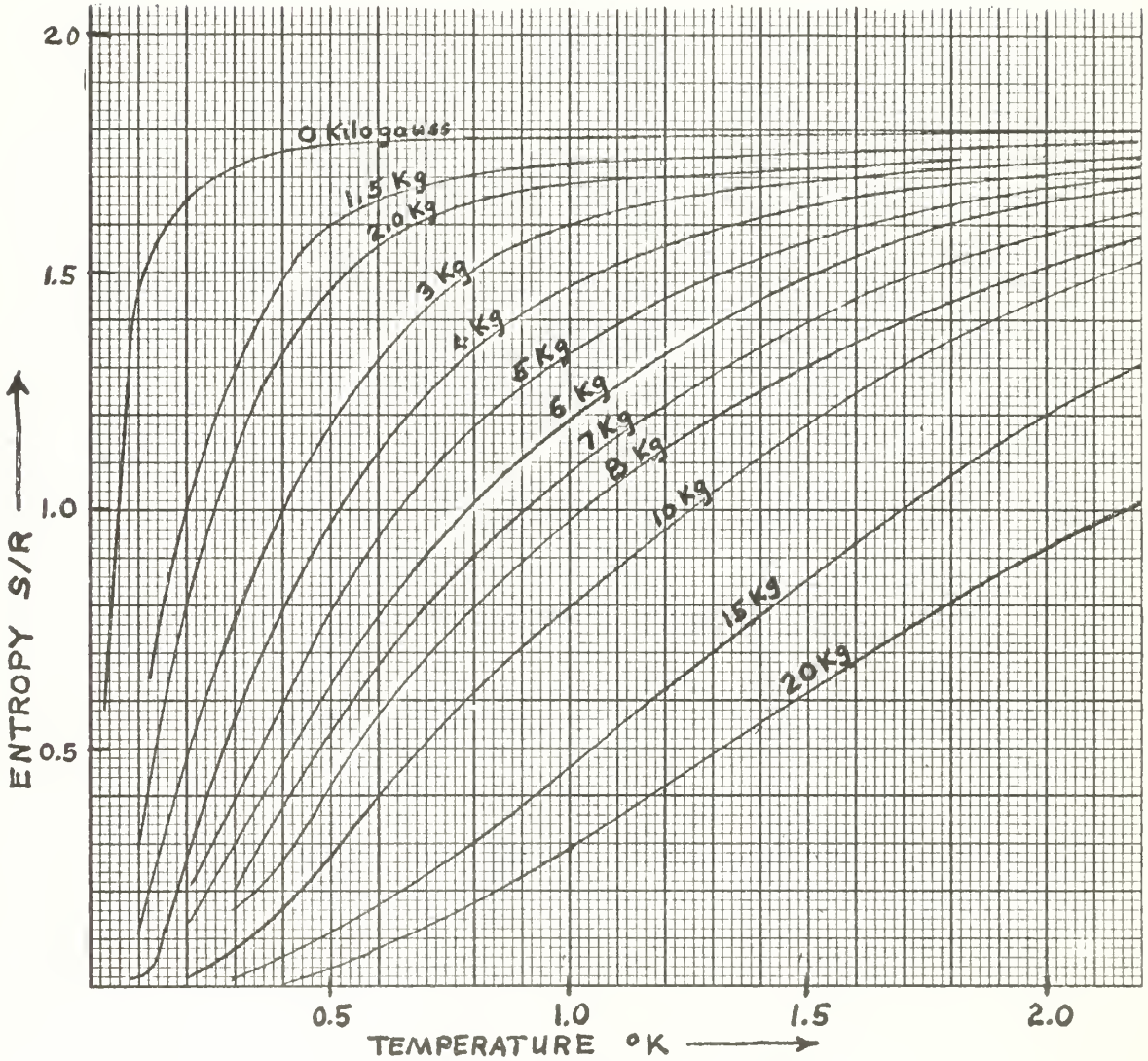

Curve below 1.2°K is taken from Heer, Barnes, and Daunt. Curve above 1.2°K is the result of extrapolation.

Therefore at 4°K

$$(S/R)_{LATTICE} = 5.5 \times 10^{-4} \times (4)^3 = 0.031$$

whereas the spin $\left(\frac{S}{R}\right) = 1.8$ at 4° $(\vec{H} = 0)$.

Using the relation given by D. de Klerk /7/:

$$(S/R)_{T<1°K} = -A(g/T^2) + B(1/T^3)$$

where:

$$A = 0.0165\ (°K)^2 \quad , \quad B = 0.00035\ (°K)^3$$

we obtain:

$$\left(\frac{S}{R}\right)_{4°K} - \left(\frac{S}{R}\right)_{1°K} = 0.015$$

for the entropy difference between 4°K & 1°K

Values for the thermal conductivity of ferric ammonium alum have been measured /8/ as:

$$k = 0.6 \times 10^{-5}\ cal/°K\ cm\ sec \quad at\ T^* = 0.07\ degree$$

and

$$k = 1.5 \times 10^{-5}\ cal/°K\ cm\ sec \quad at\ T^* = 0.10\ degree$$

where T* is magnetic temperature.

These are very low values as compared to other materials (especially metals) at the same temperature. This makes the problem of getting the "cold" out of the salt one of the major limitations on the effectiveness of the device.

The low value of thermal conductivity of the salt was the primary reason behind the decision to use a single crystal as opposed to a packed powder, as is the usual method. In addition, a higher packing density was possible with the crystal than could be obtained even from highly compressed powders.

It has been estimated /9/ that the thermal conductivity of a single

crystal of ferric ammonium alum will be from 6 to 50 times higher than that of a compressed powder at 0.1°K. (A factor of ten would be a typical average.)

Ferric ammonium alum has a fairly strong tendency to dehydrate when exposed to the atmosphere. For this reason, several precautions must be taken. The crystal must be provided with a coating which will hold up at liquid helium temperatures and be imprevious to moisture. It is proposed that as much of the crystal as possible be coated with a MYLAR film sealed in position with epoxy. (Care must be taken to insure that the heat generated in the epoxy while curing does not decompose the crystal.) GLYPTAL may also be used to help seal the crystal.

It is recommended that the crystal be kept under refrigeration when not actually in use to help prevent dehydration. Also, the crystal should be cold (below 0°C), before subjecting it to a vacuum.

With the proposed geometry, the salt will be a residual magnetic field of less than 350 gauss. Therefore, if we assume an initial temperature of 2°K, and an average field of 7.7 kilogauss from the solenoid, the salt should be able to reach a temperature as low as 0.15 K.

Annealed, 99.999% pure silver wire was selected to provide the thermal link between the maser and the salt because it had an extremely high thermal conductivity at temperatures within the device's proposed operating range (See Fig. 30). A comparably low thermal impedance could be obtained by using a much larger cross sectional area of copper conductor, as is the usual practice in magnetic cooling devices; however, by the use of the silver wire, which has a low specific heat to start with, the total heat capacity of the thermal link could be kept much lower than would be possible with a link made of any other material. The thermal conductivities of pure

FIGURE 30

THERMAL CONDUCTIVITY

OF SILVER AND COPPER

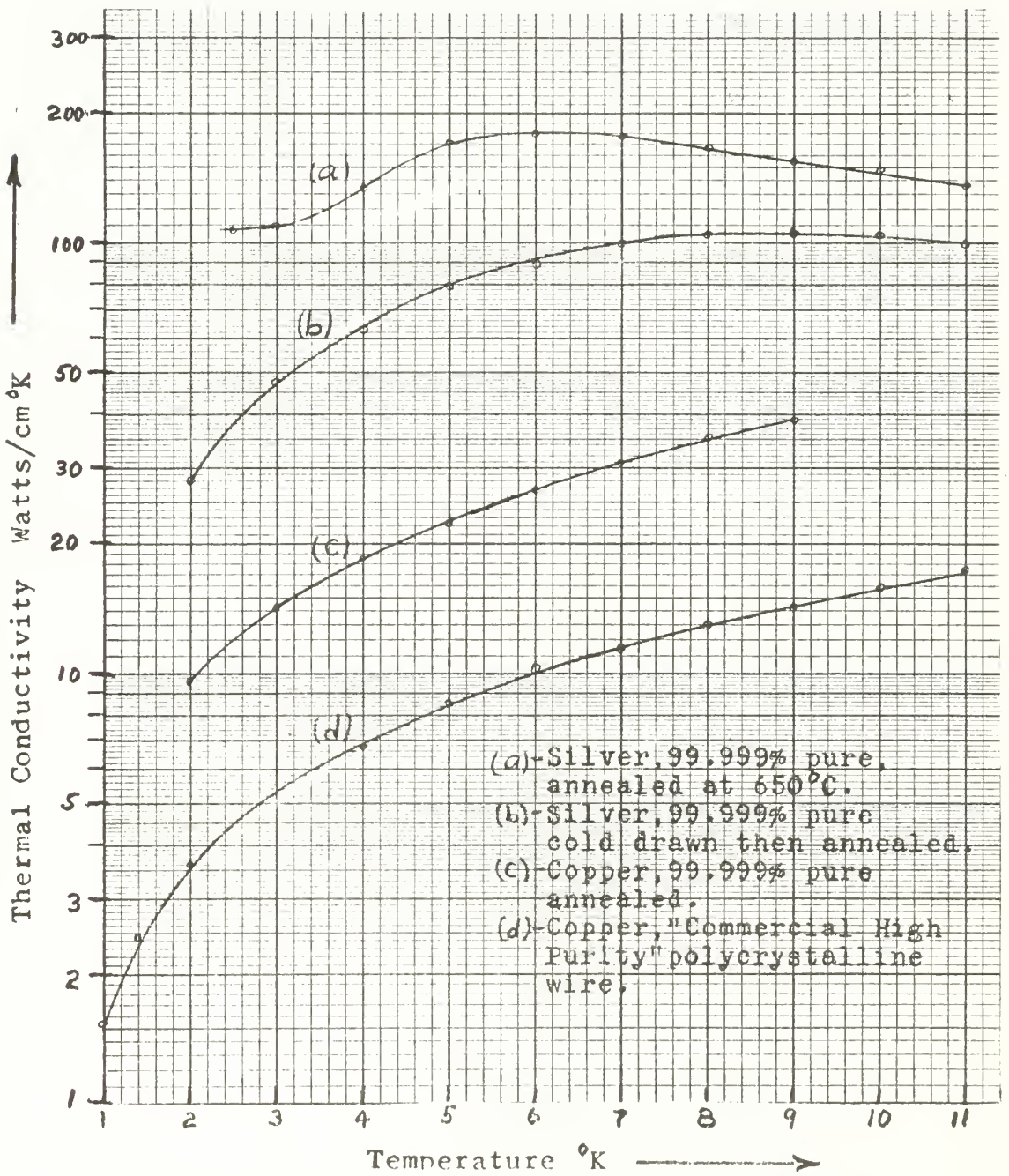

Curves are taken from National Bureau of Standards Circular #556.

silver and of copper are shown in Figure 30.

The ultra pure silver wire used for the link was obtained from Johnson, Matthey & Co., Limited; London, England, in the form of 0.020" diameter wire. The wire was cut into 39-47 cm lengths. The wires were grown into the crystal in two concentric circles, fifteen wires in a 1.75" diameter circle and the remainder in a 2.40" diameter circle. The silver wires in each circle are interconnected by 14 strands of 0.005" by 0.015" chemically pure silver ribbon to form a mesh. The wire and the ribbon are spot welded together. To help eliminate heating due to eddy currents, the silver ribbon is arranged so that it does not form a closed loop around the axis of the crystal. The use of the silver ribbon, in addition to the wire, more than doubles the surface area contact between the salt and the silver. Since the iron alum is corrosive to silver, the portion of the wires were within the crystal are coated with General Cement Insulating varnish. (GLYPTAL would also have been satisfactory.)

Since the time alloted for this project was quite short, the overall device has never been tested and there are several unsolved problems at the time of this writing.

The ferric ammonium alum crystals sometimes undergo fracturing at liquid nitrogen temperatures. Whether this will adversely affect the device remains to be seen.

The method of mounting the crystal has not been studied in detail; but, it appears that hanging it by a means of a MYLAR sheet wrapped around the crystal offers the greatest promise at this time. Caution must be taken to isolate the crystal from vibration, since this can cause noticeable internal heating of the crystal.

The power supply used for the magnet will probably need additional filtering to help prevent eddy current heating in the silver grids inside the crystal due to "ripple" in the magnetic field.

APPENDIX VII

CRYSTAL GROWING

Crystals of Ferric Ammonium Alum tend to grow in the shape of an equalateral octahedron. (i.e. $\{111\}$ faces dominate the crystal.) On occasions, especially on a small crystal the $\{100\}$ faces will also be prominent, but as the crystal grows the $\{111\}$ faces will dominate.

For the project, a 2.8" diameter 3-1/2" long cylinder is needed. This requires that ℓ = 14 cm. (Fig. 31).

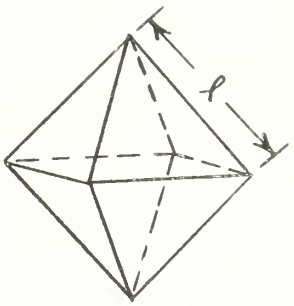

Fig. 31

$$\text{Volume} = 0.471\,\ell^3 = 1292\ \text{cm}^3$$

$$\text{Mass} = M = 1.71\ \frac{gm}{cm^3} \times 1292$$

$$= 2.21\ \text{Kg.}$$

Assuming the rate of growth is proportional to the surface area (i.e., area $\propto \ell^2 \propto M^{2/3}$), we get the formula for the growth rate as:

$$\frac{dM}{dt} = kM^{2/3}$$

where k = growth rate constant in units of $M^{1/3}/t$

Therefore, the time required to grow a crystal to a mass M is

$$t = \frac{3}{k}\left(M^{1/3} - M_0^{1/3}\right)$$

Where Mo is the mass of the seed crystal and t,k, &M are in consistent units.

The crystals were grown in a slightly supersaturated aqueous solution.

The first method of growing the crystals consisted of suspending a seed crystal in a beaker containing a saturated solution (1.244 Kg of salt

per liter of water at 20°C) with a layer of finely ground salt in the bottom. This method resulted in crystals with very few visible flaws. A growth rate with k as high as 0.014 $\frac{\text{grams}^{1/3}}{\text{hour}}$ could be maintained if the salt in the bottom of the beaker was recrushed daily, and if the solution was heated about 5°C, above room temperature and then allowed to come to saturation before replacing the crystal.

Another apparatus was devised using the U tube principle of Kruger and Finke as described by H. E. Buckley /4/. This device resulted in an average growth rate of twice that of the first system; however, the visible flaws were also noticeably increased.

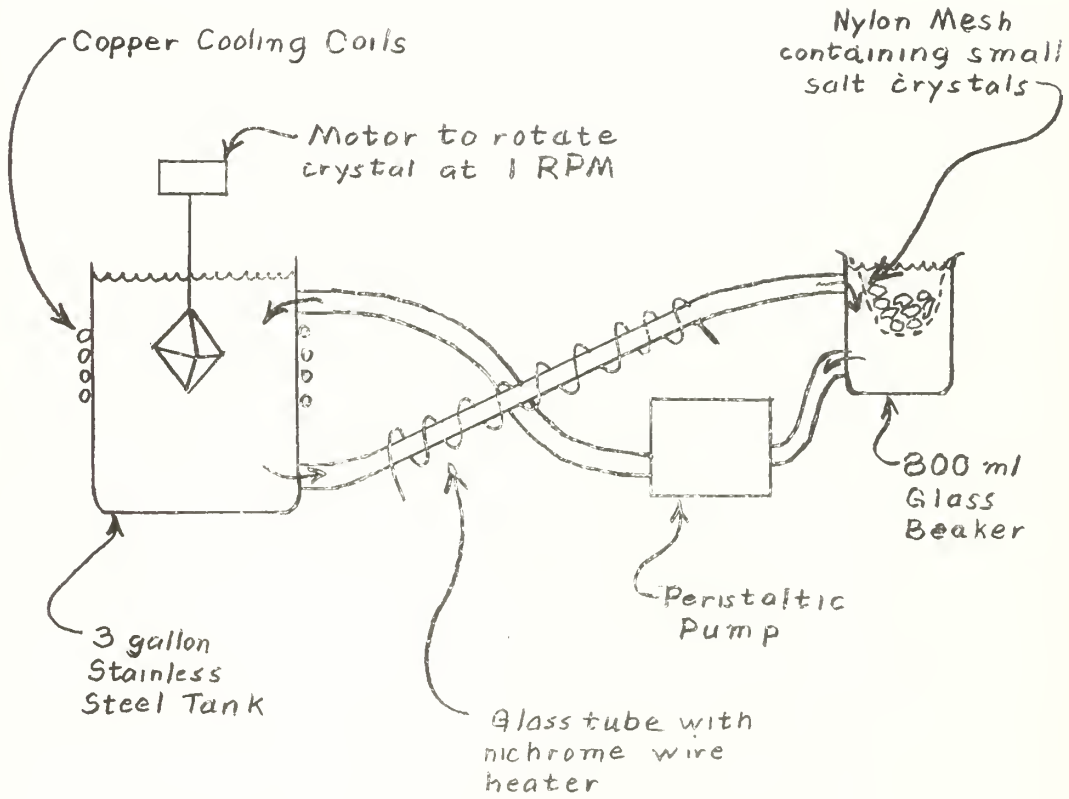

Fig. 32

The large tank was cooled by tap water flowing through copper coils wound around it. This maintained the tank at about 18°C.

Heat, to provide a temperature difference between the growing tank and the supply tank, was provided by a nichrome wire wound around a 1/2" I.D. glass tube which carried the flow of solution from the growing tank to the supply tank. The tube was insulated with asbestos paper. The temperature difference in the tanks was regulated by controlling the current through this heater.

The supply tank consisted of a 800ml glass beaker with 2-1/2" I.D. glass stubs welded onto it. The supply of salt was suspended in the solution using a piece of nylon mesh.

At first, a reflex condensor was used in the other link between the tanks to provide cooling. The motive force for circulation was provided by gravity. This system was impractical since the condensor would clog up daily with salt crystals. The condensor was then replaced by a peristaltic pump which provided a flow of about 100cc/min.

The crystal was rotated in the growing solution at a rate of 1 RPM.

With a temperature difference between the tanks of 6 to 8°C., a growth rate of $k = 0.06\ g^{m^{1/3}}/hr$ was obtained; however, this resulted in extremely poor crystals. They were soft and had a high degree of water inclusion as could be seen by their brown color as opposed to the normal pale violet color of a good crystal.

By dropping the temperature difference to approximately 2°C., a growth rate of k = 0.025 to 0.03 $g^{m^{1/3}}/hr$ was obtained. The crystals had very little water inclusion but did have a number of noticeable flaws.

Several crystals of approximately 1kg mass were grown using this method.

This system would require cleaning about once every three days.

Several attempts were made to change the mode of growth from {111} faces to {100} faces by regulating the pH but were all unsuccessful.

The seed crystals were suspended by waxed cotton thread or cord. Nylon cord would not hold up in the solution. The seed for the crystal to be used in the adiabatic demagnetization device consisted of 2 - 200 gram single crystals that were drilled and mounted on a 1/4' steel rod.

The salt solution was very corrosive to most materials, especially metals. Stainless steel was about the only metal that would hold up in the solution. Copper and iron were attacked with noticeable vigor with most of the reaction occurring at the liquid-air interface.

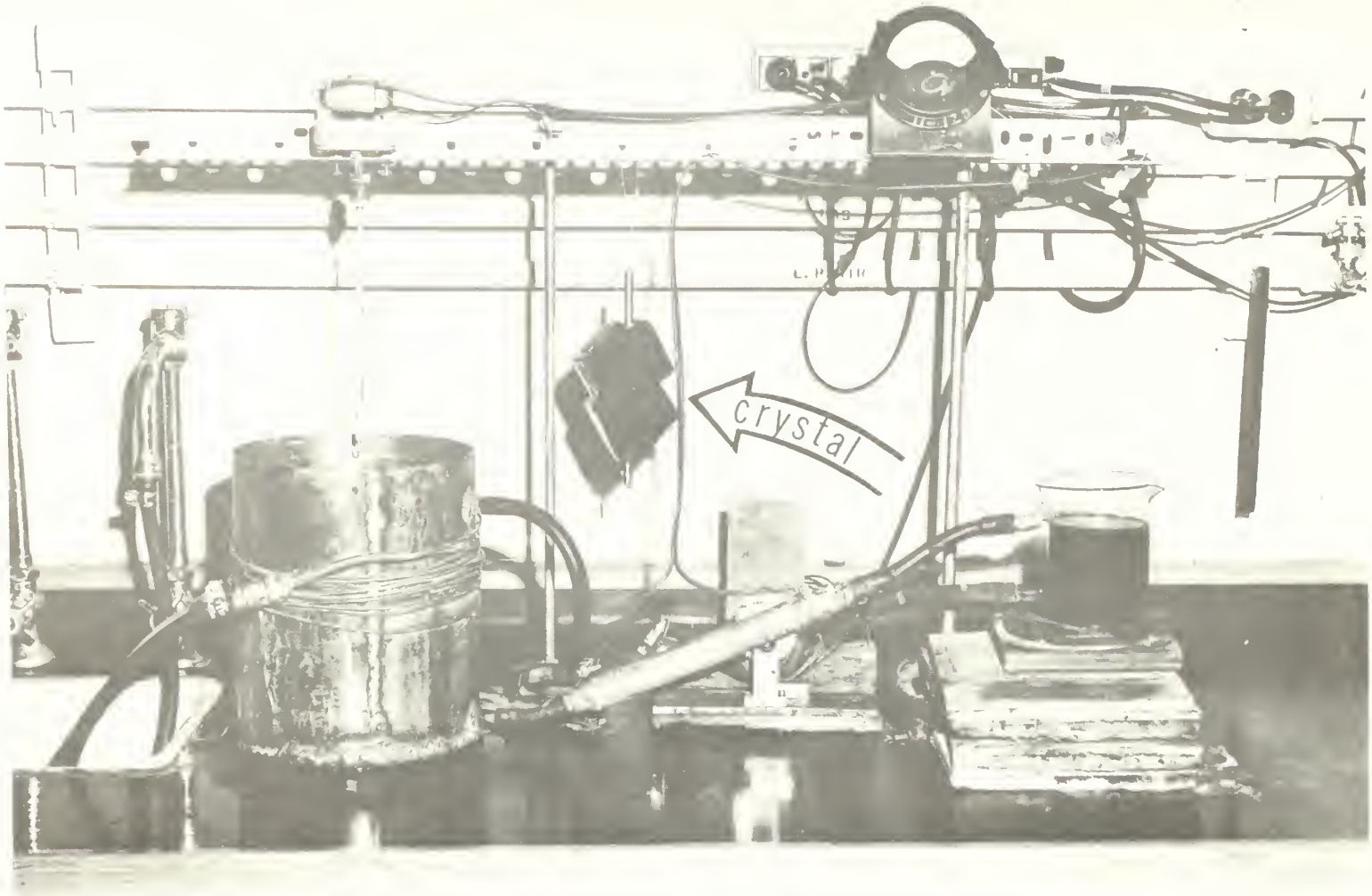

Figure 33. The Crystal Growing Apparatus

BIBLIOGRAPHY

1. Boom, R. W., and R. S. Livingston, Superconducting Solenoids, Proceedings of the IRE, 50, p 274 (March, 1962)

2. Montgomery, D. B., Current-Carrying Capacity of Superconducting Nb-Zr Solenoids, Applied Physics Letters, 1, p 41, (October, 1962)

3. Sobol, M., and J. J. McNichol, Evaporation of Helium I Due to Current-Carrying Leads, The Review of Scientific Instruments, 33, p 473 (April 1962)

4. Buckley, H. E., Crystal Growth, John Wiley and Sons, Inc., p 49 (1951)

5. Heer, C. H., C. B. Barnes, and J. G. Daunt, Magnetic Refrigerator for Maintaining Temperatures below 1°K, Physics Review, 91, p 412 (1953)

6. Garrett, C. G. B., Magnetic Cooling, Harvard University Press, p 23 (1954)

7. deKlerk, D., Adiabatic Demagnetization, Encyclopedia of Physics, XV, Low Temperature Physics II

8. Kurti, N., B. V. Rollin, and F. E. Simon, Preliminary Experiments on Temperature Equilibria at Very Low Temperatures, Physica, 3, p 266 (1936)

9. Ambler, E. and R. P. Hudson, Magnetic Cooling, Reports on Progress in Physics, XVII, p 280 (1955)

10. Graham, A. K., Electroplating Engineering Handbook, Reinhold Publishing Corp., 2nd edition, p 205-207 (1962)

11. Scott, R. B. Cryogenic Engineering, D. Von Norstrand Co., Inc., p 333 (1959)

12. Radio Amateur's Handbook, American Radio League, p 27 (1956)

13. Henny, K., Radio Engineering Handbook, McGraw-Hill, p 3.19-3.19 (1959)